INSTITUTE OF PHYSICS PUBLISHING PHYSIOLOGICAL MEASUREMENT

Physiol. Meas. **27** (2006) R63–R108 doi:10.1088/0967-3334/27/12/R01

TOPICAL REVIEW

Scanning electrochemical microscopy: principles and applications to biophysical systems

Martin A Edwards, Sophie Martin, Anna L Whitworth, Julie V Macpherson and Patrick R Unwin

Department of Chemistry, University of Warwick, Coventry CV4 7AL, UK

E-mail: P.R.Unwin@warwick.ac.uk

Received 20 April 2006, accepted for publication 18 September 2006
Published 17 October 2006
Online at stacks.iop.org/PM/27/R63

Abstract

This review highlights numerous and wide ranging biophysical and biochemical applications of scanning electrochemical microscopy (SECM). SECM instrumentation and theoretical modelling, necessary for experimental interpretation, are outlined, followed by a detailed discussion of the diverse applications of this technique. These include the measurement of flow through membranes, the determination of kinetic parameters of reactions, the investigation of the permeability of small molecules in tissues and monitoring biological processes, such as the production of oxygen or nitric oxide by cells. The significant impact of micro-electrochemical techniques on our understanding of basic physicochemical processes at biologically relevant interfaces is also considered. Studies reviewed include transport across and within bilayers and monolayers. Recent advances in SECM include the combination of SECM with other techniques, such as atomic force microscopy and optical microscopy. These developments are highlighted, along with prospects for the future.

Keywords: scanning electrochemical microscopy, bilayers, monolayers, scanned probe microscopy, interfaces, electrochemistry, mass transport

(Some figures in this article are in colour only in the electronic version)

1. Introduction

Scanning electrochemical microscopy (SECM; the same acronym is used to describe the instrument) has developed into a powerful technique for quantitative investigations of interfacial physicochemical processes, in a wide variety of areas, as considered in several recent reviews (Barker *et al* 1999, 2001, Mirkin 1999, Amemiya *et al* 2000, Mirkin and

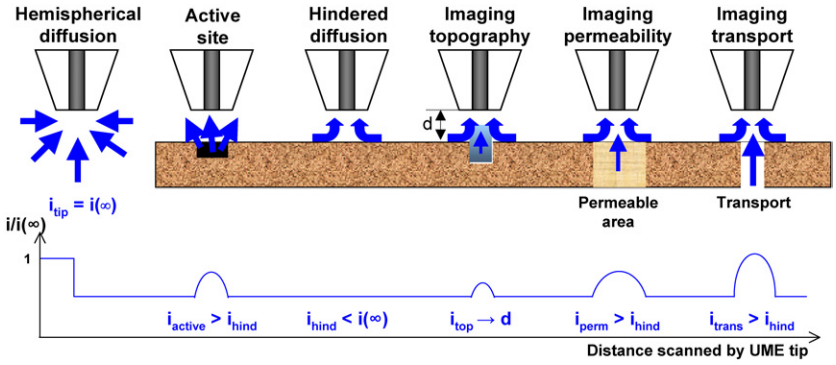

Figure 1. A selection of modes of operation of a SECM, illustrating how the current response, expressed as a normalized quantity (see the text), changes upon imaging certain features. Arrows represent the flow of the electroactive species (or ions) to the UME.

Horrocks 2000, Yasukawa *et al* 2000b, Gyurcsányia *et al* 2004, Pu *et al* 2005). This review will provide a background to SECM, with particular reference to its use in characterizing biophysical processes and biomaterials.

In the simplest terms, SECM involves the use of a mobile ultramicroelectrode (UME) probe, either amperometric or potentiometric, to investigate the activity and/or topography of an interface on a localized scale. The attractive features of SECM, for the study of biomaterials on a local scale, were recognized soon after the technique was formally established (Bard *et al* 1989, Kwak and Bard 1989a, 1989b). Early applications included quantitative studies of immobilized enzyme activity (Pierce *et al* 1992, Pierce and Bard 1993, Shiku *et al* 1995, 1996, 1997) and photosynthetic processes on leaves (Lee *et al* 1990, Tsionsky *et al* 1997b). These studies provided the foundations for the expansion into many new areas, as described in this review. These include the investigation of transfer processes, such as the passage of small molecules, e.g. oxygen, across biomimetic membranes (lipid bilayers and monolayers), and mapping the micron-scale porous nature of dentine or the sub-micron pores in membranes. Also included herein are applications that examine cellular activity and respiration and its variance with conditions (metastatic breast cancer cells, protoplasts and embryos), and studies of the permeability of oxygen in cartilage. SECM is able to resolve differences on the micron or sub-micron length scale, an advantage which is clear in the aforementioned examples and in many other biological situations.

We begin with a basic overview of the principles and instrumentation for SECM, introduce the modelling techniques needed to understand the underlying processes and analyse experimental data, before considering specific methods and applications. We conclude with a brief overview of very recent developments and potential future developments, including hybrid techniques that involve SECM and the study of processes at the single-cell level.

Several modes of SECM have been developed to allow the local chemical properties of interfaces to be investigated. A comprehensive review of all of the techniques can be found in Bard and Mirkin (2001). Figure 1 demonstrates the wide ranging information that can be extracted from the current of an amperometric UME, used as the probe in SECM. The arrows represent the flux of a redox-active species (or ion in the case of a microcapillary probe; see section 2.3.5 on micro-ITIES probes) to the UME. These examples will be developed further in section 4.

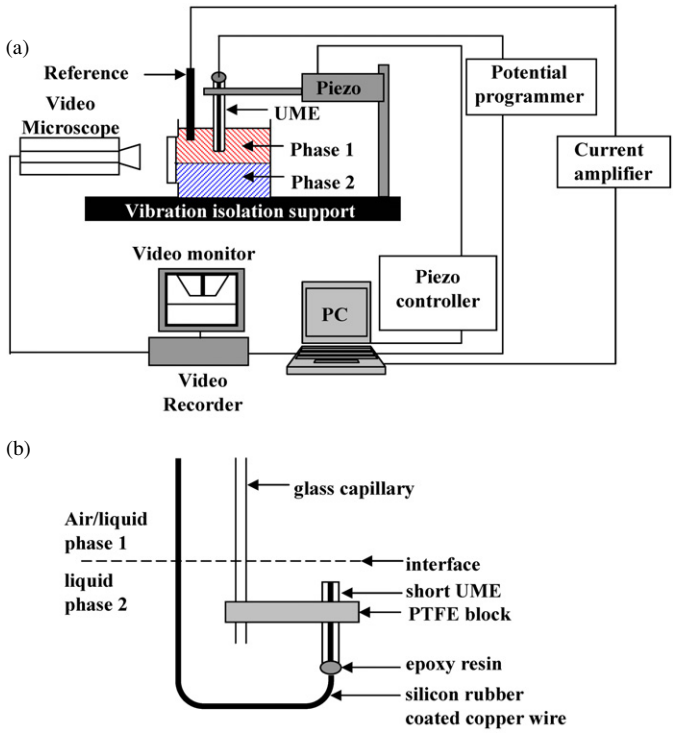

Figure 2. Schematic views of (a) a rig, for SECM, and (b) a submarine electrode.

2. Instrumentation

Although commercial instruments for SECM are available from several companies, including CH Instruments (USA), Windsor Scientific (UK) and Uniscan (UK), many instruments are still constructed by individual research groups; these are then tailored to specific applications. At the heart of SECM is the amperometric or potentiometric tip, whose location is controlled remotely, with appropriate positioners, relative to the sample interface. The type of experimental cell or vessel in which measurements can be made ranges from a simple beaker (Zhang *et al* 2000) to a Langmuir trough in a controlled atmosphere (Slevin *et al* 1998, Slevin and Unwin 2000). Electrochemical control and measurement in SECM is relatively simple as discussed in the next section.

2.1. Electrochemical instrumentation

For amperometric control of the tip, with externally unbiased interfaces, a simple two-electrode system suffices (figure 2(a)). A potential is applied to the tip, with respect to a suitable reference electrode, to drive the process of interest at the tip and the corresponding current that flows is typically amplified by a current-to-voltage converter. If the sample is also to be biased externally, a bipotentiostat is required. For some studies of membrane transport, ion flow is driven from a donor to receptor compartment galvanostatically, and a potentiostatically controlled tip serves as a detector (Bath *et al* 2001). Potentiometric detection with UMEs

of various types is readily accomplished (Amman 1986, Wei *et al* 1995), typically using a voltage follower with an input impedance appropriate to the type of indicator electrode used.

2.2. Positioning

The tip is attached to positioners, which allow it to be moved and positioned relative to the interface under investigation. A variety of positioners have been employed in SECM instruments, with the choice depending on the type of measurement and spatial resolution required. For the highest (nanometre) resolution, piezoelectric positioners similar to those used in scanning tunnelling microscopy (STM) are mandatory (Liu *et al* 1986). There has also been some use of stepper motors to control the position of the tip in the x–y plane (Kranz *et al* 1995a, 1995b, Hliva *et al* 1998), parallel to the interface of interest.

In the application of SECM at solid/liquid interfaces (section 4.1), high-resolution x, y, z positioning and scanning is usually required. However, many SECM measurements, e.g. at air/liquid interfaces (section 6.1.2), simply involve the translation of a tip towards and/or away from a specific spot on an interface, in the perpendicular (z) direction. In this situation, it is only necessary to have high-resolution z-control of the tip, typically using a piezoelectric positioner, while manual stages suffice for the other two axes (Slevin *et al* 1996, Barker *et al* 1998). It has further been shown that SECM measurements can be made with manual stages on all axes, with the z-axes driven by a differential micrometer and the x–y stages controlled by fine adjustment screws. This simple cost-effective set-up allows tip approach measurements to be made with a spatial resolution of ± 0.25 μm (Martin and Unwin 1997, 1998b). The use of a video microscope, aligned such that the electrode may be observed from the side, has proved useful in facilitating the positioning of the UME probe relative to the interface of interest (Slevin *et al* 1996, Barker *et al* 1998).

2.3. Probes

The type of probe electrode used in SECM depends on the particular process under investigation. A diversity of probes is available for amperometry and potentiometry. Since these often have to be prepared in house, we highlight some of the most important tip designs in this section. In-depth reviews of UME design, fabrication and characterization can be found in Zoski (2002) and Forster (2003).

2.3.1. Micron-sized disc-shaped electrodes sealed in glass. Typically, amperometry involves electrolysis at a solid UME, usually a disc-shaped electrode, with a diameter of 0.6–25 μm. This type of electrode is readily fabricated by sealing a wire of the material of interest, in a glass capillary, making an electrical connection and polishing the end flat; see figures 3(a) and (b) for illustrations of such an electrode (Bard *et al* 1989, 1993, Wightman and Wipf 1989). Pt, Au and C electrodes have been successfully fabricated in this way. For most SECM studies, the ratio of the diameter of the tip (electrode plus surrounding insulator, $2r_s$) to that of the electrode itself, $2a$, RG $= r_s/a$ is typically around 10. This minimizes effects from back diffusion (from behind the probe), making the electrode response more sensitive to the surface process.

SECM images may be convoluted with both activity and topographical contributions. To resolve such effects, it may be possible to scan the sample twice, with the mediator of interest and then with a moiety that is inert with respect to the sample, so mapping the topography (Gonsalves *et al* 2000a, 2000b). Dual amperometric probes with one channel serving as a topographic sensor and the other to determine activity have also been crafted

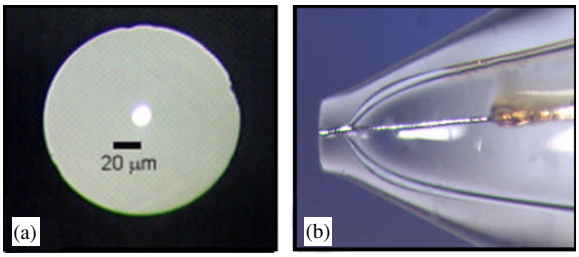

Figure 3. Optical microscope images: (a) normal disc UME (top view); (b) normal disc UME (side view).

(Yasukawa *et al* 1999a). Such probes have found application for dual potentiometric–amperometric/conductivity sensing (Wei *et al* 1995), as described in section 2.3.6 Other solutions to the problem of deconvoluting topographic and activity components of an image can be found in sections 5.1 (shear force feedback), 5.2 (tip position modulation—TPM) and 2.3.4 and 5.3 (combined SECM–AFM (atomic force microscopy)).

2.3.2. Submarine probes. For some liquid/liquid interfaces and for studies at the water/air interface, a 'submarine' electrode can be deployed (Slevin *et al* 1996, 1997, 1998), depicted schematically in figure 2(b). In this case, the electrode is inverted in the cell, such that the tip points upwards and an insulated connection is made through the solution.

2.3.3. Sub-micron- and nanometre-scale electrodes. To improve the spatial resolution of SECM, there is much interest in reliable methods for shrinking the size of the probe electrode. Probably, the simplest approach is to electrochemically etch a length of metal microwire to a sharp point and insulate off all but the end of the probe, leading to a conically shaped tip. This methodology is often employed in the fabrication of electrochemical scanning tunnelling microscopy tips. A number of different coating procedures have been investigated, such as a simple dipping technique with a varnish (Gewirth *et al* 1989) or molten paraffin (Zhang and Wang 1994). Translation of the tip through a molten bead of glass (Penner *et al* 1989, 1990), poly(α-methylstyrene) (Penner *et al* 1989) or apiezon wax (Nagahara *et al* 1989) held on a heated support has also been adopted as a method for applying an insulating coating to etched metal wires.

The electrophoretic deposition of an insulating polymer film is a popular choice for coating tips (Potje-Kamloth *et al* 1989, Bach *et al* 1994, Slevin *et al* 1999, Conyers and White 2001). In this case, shrinkage of the polymer coating from the tip end, during curing at high temperature, results in the formation of a sub-micrometre-sized electrode. Full details on this fabrication strategy are given elsewhere (Bach *et al* 1994, Conyers and White 2001).

Several groups have worked on the production of tiny disc-shaped UMEs, sealed in glass (Pendley and Abruña 1990, Shao *et al* 1997, Ballesteros-Katemann and Schuhmann 2002). Electrodes of this type are fabricated by heating and pulling metal wires inserted into quartz or borosilicate glass capillaries. As the glass is drawn out, the metal thins, resulting in the formation of a needle-shaped electrode. A detailed procedure for producing this type of tip with a high yield has been described by Schuhmann's group (Ballesteros-Katemann and Schuhmann 2002). Very recently, White's group has described a procedure for sealing an etched wire in glass to produce well-defined disc-shaped electrodes with sub-100 nm diameter (Zhang *et al* 2004, Rudd *et al* 2005).

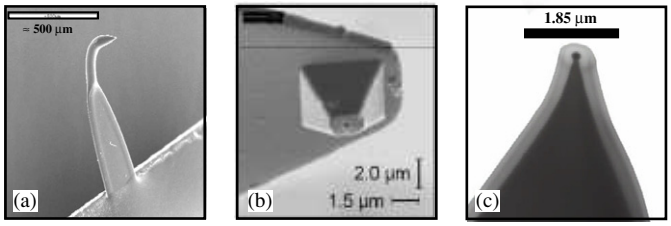

Figure 4. Scanning electron micrographs of (a) a typical hand-fabricated SECM–AFM probe, (b) an integrated frame microelectrode and (c) the tip of a nanowire SECM–AFM probe. (Part (b) reprinted in part with permission from Sklyar *et al* (2005), copyright 2005 American Chemical Society.)

As the electrode dimensions shrink, characterization of the probe geometry becomes more challenging. High-resolution imaging techniques, such as scanning electron microscopy, are often needed, in conjunction with voltammetry and SECM approach curve measurements, where the tip feedback current is recorded as a function of distance, d, from either an inert interface or conducting surface. The shape of the curve is characteristic of the probe geometry (Davis *et al* 1987, Kwak and Bard 1989b, Mirkin *et al* 1992, Selzer and Mandler 2000).

2.3.4. SECM–AFM probes. A recent development in scanning probe design has been the combination of atomic force microscopy (AFM) with SECM. AFM maps the topography of a substrate with nanometre vertical resolution, by monitoring the interaction force between the sample and a sharp tip, that is attached to the end of a force-sensing cantilever (Binnig *et al* 1986, Rugar and Hansma 1990, Wiesendanger 1994). By integrating an electrode into the AFM probe design, it is possible to obtain both electrochemical and topographical information, thus enabling structure–activity-related problems to be addressed at high spatial resolution. The size of the electrode is of paramount importance and this should be in the micron or sub-micron range (spatial resolution of the electrochemical response scales with electrode dimension). Alternatively, one can use the electrode component of a SECM–AFM probe to induce a topographical change, such as the dissolution or growth of a surface (Macpherson *et al* 1996, Jones *et al* 2000, 2003), which can then be tracked through the AFM component of the instrument.

To date, several approaches to fabricating SECM–AFM probes have been devised. The first employs hand-fabricated probes produced by coating an etched and flattened microwire with an electrophoretic paint (Macpherson and Unwin 2000, 2001). The flattened section provides a flexible cantilever (force sensor), and the coated etched tip acts as an electrode (figure 4(a)). SECM–AFM probes with conically shaped electrodes of size 10–1000 nm have been fabricated in this way. The probes can be used in conjunction with any commercially available AFM instruments. These probes have also been used to image the conductivity of heterogeneous surfaces (Macpherson and Unwin 2001). While this fabrication procedure is simple, each probe is necessarily different and the topographical capabilities of the probes are not of the quality of commercial AFM tips.

A second method employs a conventional AFM probe as the starting platform. Electrochemical capability is built into the device by sputtering or evaporating a thin metal film (typically Pt) onto the AFM probe (Macpherson *et al* 1996, Jones *et al* 1999). The body of the probe is insulated, leaving the exposed cantilever as the electrode (typical length 100–200 μm, width 20–40 μm) (Macpherson *et al* 1996, Jones *et al* 1999). This type of probe has found particular applications for inducing and imaging dissolution processes (Macpherson

et al 1996, Jones *et al* 2000, 2003). Unless imaging a substrate in air (Macpherson *et al* 2002), one cannot use this type of probe for high-resolution electrochemical imaging.

As an alternative to the previous method, one can insulate the entire probe, then expose the electrode, for example, through shaping and remodelling the original AFM tip using a focused ion beam (FIB) (Kranz *et al* 2001). This approach leaves a small electrode area, facilitating electrochemical measurements and imaging at high spatial resolution (figure 4(b)), but again each probe is typically fabricated and characterized on an individual basis.

Most recently, ultrahigh-resolution imaging probes have been developed by attachment of single-walled carbon nanotubes to the tip of a metal-coated AFM tip and using these as a template for the deposition of a metal nanowire (Burt *et al* 2005b). The whole probe is finally insulated and the end of the nanowire is cut by a FIB. The resulting electrode has a well-defined disc geometry, the size and composition of which can be controlled easily with typical diameters being 50–100 nm. Figure 4(c) shows the tip of a nanowire probe (Burt *et al* 2005b).

A recent advance in SECM–AFM is the development of a batch procedure for the fabrication of probes. Using electron beam lithography, it has been possible to produce probes of a reproducible nature from a silicon wafer (Dobson *et al* 2005). This methodology offers great promise for the fabrication of many probes at a time which have similar characteristics and further work to develop batch procedures and a range of probe electrode geometry would undoubtedly lead to an uptake of the SECM–AFM technique. SECM–AFM has been reviewed by Gardner and Macpherson (2002) and some applications of SECM–AFM are considered further in section 5.3.

2.3.5. Micro-ITIES probes. As mentioned in section 1, amperometry is not limited to electron transfer reactions between a metal electrode and a redox moiety. Considerable research has been carried out on electron transfer and ion transfer at the polarized interface between two immiscible electrolyte solutions (ITIES) (Liu and Mirkin 2001, Guo *et al* 2004). Girault's group first demonstrated that amperometric ion transfer measurements could be made at a liquid/liquid interface formed at the opening of tapered glass capillary (Osborne *et al* 1994). These probes are made by filling a tapered pipette containing a metal counter electrode with one liquid (water or organic solvent) and placing it into a second immiscible phase containing a second (counter-reference) electrode. The successful deployment of this type of probe in SECM has expanded the range of species that can be detected (Solomon and Bard 1995, Shao and Mirkin 1997).

Both electron transfer and ion transfer processes can be driven at a micro-ITIES probe by polarizing the interface formed between the liquid in the capillary and the immiscible solution into which the probe is placed. For example, electron transfer between the reduced form of an aqueous redox couple, at a high concentration in a capillary, and the oxidized form of a second redox couple in an organic solution has been demonstrated (Solomon and Bard 1995). The voltammetry at this type of polarized ITIES is similar to that at a metal UME, with the current ultimately governed by the diffusion of the species in the organic phase, provided that the aqueous couple is at a sufficiently high concentration relative to that in the organic phase. The use of a polarized ITIES to induce ion transfer provides a route for injecting or depleting specific ions, such as K^+ (Shao and Mirkin 1997, Amemiya and Bard 2000, Evans *et al* 2000), on a local scale close to a target interface.

2.3.6. Potentiometric probes. The simplest potentiometric probes are made from metal discs sealed in glass capillaries or an insulating polymer sheath, prepared in a similar way to the

amperometric tips described above. For example, silver and silver chloride coated disc-shaped UMEs have found application in the potentiometric monitoring of Ag^+ and Cl^- (Denuault *et al* 1992, Kemp *et al* 1995). Nanometre-scale versions of these UMEs can be fabricated from etched wires (Gray and Unwin 2000, Eftekhari 2001) or by pulling a metal wire inside a glass capillary, as described in section 2.3.3 (Shao *et al* 1997). Antimony UMEs have also proved to be a powerful pH probe over the pH range 5–9 (Horrocks *et al* 1993). Advantages of these electrodes are that they are easy to make and have a fast response time. Moreover, such probes can be used in amperometric as well as potentiometric mode, opening up the possibility of determining tip–interface distances (from the hindered diffusion, negative feedback mode, described in section 4.2).

Liquid membrane glass micropipette based ion-selective UMEs expand the range of species detectable by potentiometry and have found considerable general application in the life sciences (Amman 1986). There are, however, specific considerations when employing such probes in SECM. In particular, it is difficult to fabricate electrodes that allow high (micrometre or sub-micrometre) spatial resolution and have a fast response time. Ion-selective UMEs for K^+, NH_4^+ and Zn^{2+} have been fabricated (diameters in the range 1–20 μm (Wei *et al* 1995)), with response times that allow tip scanning at 10 μm s^{-1}. These UMEs comprise a selective liquid membrane in the end of a pulled capillary, which separates an internal reference solution from an external test solution containing the second reference electrode. The potential developed between the two electrodes is used to determine local concentration perfusing to the tip. Among the range of potentiometric probes of this type, a pH-sensitive electrode is particularly noteworthy (Klusmann and Schultze 1997).

It is important that the absolute distance between the UME and the interface is known, both to avoid tip crashes and to ensure that quantitative information about near-interface concentrations can be obtained. In this case, dual tip sensors have been developed, with a potentiometric indicator electrode and a second sensor which monitors the distance. This type of double-barrel electrode has employed either conductivity or amperometry to maintain the tip-to-sample separation (Wei *et al* 1995).

2.4. Cells

A wide variety of SECM cells have been developed to accommodate the diversity of interfaces and applications. Detachable cells are particularly useful, as they allow ready exchange between different types of samples. These are typically manufactured from inert plastics or glass, having access holes/windows for various electrodes, gas/fluid lines or cameras, as the experiment requires. Solid substrates are fixed to the base of the cell such that they are normal to the cylindrical axis of the UME.

A convenient way to study membranes, which effectively separate a donor solution from a receptor solution, is to mount the membrane of interest on the end of a glass capillary and insert this vertically through a hole drilled in the cell base, so that the membrane lies perpendicular to the tip axis. The other end of the tube is then connected to a reservoir, containing the donor solution. This simple set-up allows the study of transmembrane transport by convection (with a hydrostatic or osmotic pressure across the membrane), diffusion (with a concentration difference between the donor and receptor phases) and ion migration (with a potential applied across the membrane).

The integration of SECM with a Langmuir trough to permit the study of monolayers at water/air (W/A) interfaces is an area of considerable promise (Slevin *et al* 1998, Slevin and Unwin 2000, Zhang *et al* 2001, Cannan *et al* 2004, Ciani *et al* 2004, Burt *et al* 2005a). In this case, a submarine UME (figure 2(b)) controlled remotely by appropriate micropositioners

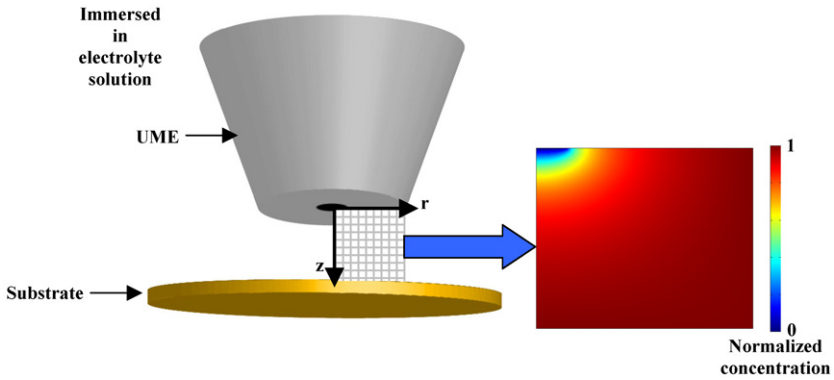

Figure 5. Simulation of normalized concentration at an UME generated by Comsol Multiphysics (right) with two-dimensional symmetry of system schematically illustrated (left).

is deployed in the dipping well of a conventional Langmuir trough and used to approach the water/air interface.

3. Modelling

The interpretation of SECM experimental results typically requires the formulation of a model of the process being investigated. The model is informed by knowledge of the physicochemical process of interest and experimental data. Experimentally, typically only current or potential is measured (as a function of probe position and sometimes time); from these measurements one seeks to determine transport phenomena and/or reaction kinetics. The careful design of experiments and formulation of underlying models is thus imperative. In this section, we briefly highlight methods commonly used for SECM modelling.

Many of the recent numerical approaches for solving the differential equations describing mass transport in microelectrode problems mirror those used in engineering to treat fluid flow (Johnson 1998) and heat transfer (Hewitt *et al* 1997), namely finite-element methods (FEMs) (Huebner and Thornton 1982, Rao 1982) or finite-difference methods (FDMs) (Feldberg 1972). In the application of these approaches to electrochemical problems, the continuous diffusion field (concentration as a function of space and time) is described in terms of discrete values at prescribed locations, e.g. at the nodes of a grid dissecting the diffusion field.

The first treatment of mass transfer in the SECM geometry used the FEM to calculate the steady-state tip current response and concentration profile, for an UME operating in the SECM feedback mode positioned close to an infinite, planar, conducting or inert substrate (Kwak and Bard 1989b).

The alternating direction implicit finite-difference method, ADIFDM, has also been employed extensively as an efficient digital simulation technique for solving two-dimensional time-dependent problems (two-dimensional reduction of problem illustrated in figure 5). This was first used to simulate the SECM feedback response for the case where the tip-generated species undergoes homogeneous chemical reaction in solution (Unwin and Bard 1991). The method was subsequently employed to model the SECM feedback mode with heterogeneous kinetics for infinite and arbitrary-sized substrates (Bard *et al* 1992). Since these initial applications, ADIFDM has been used to model a variety of kinetic situations for several different SECM modes, incorporating heterogeneous (Pierce *et al* 1992, Unwin and Bard

1992, Macpherson and Unwin 1994, 1995a, 1995b, 1996, Slevin *et al* 1997) or homogeneous (Zhou *et al* 1992, Demaille *et al* 1996, Martin and Unwin 1998a) kinetics.

The effect on the SECM chronoamperometric response of allowing the two redox forms of a couple to have arbitrary diffusion coefficients has been assessed through model calculations using the ADIFDM, for the positive feedback (section 4.3.1) (Martin and Unwin 1997) and generation/collection (Martin and Unwin 1998b) modes and for the reverse transient behaviour of SECM double potential step chronoamperometry (DPSC) (section 6.1.2.1) measurements in bulk solution (Macpherson and Unwin 1997).

A comprehensive theoretical treatment of SECM-induced transfer (SECMIT; see section 4.3.2) occurring between two phases is offered in Barker *et al* (1998). The parameter space characterized by the partition coefficient of the solute, K_e, the relative diffusion coefficients of the solute in the two phases, γ, and the interfacial transfer kinetics has been explored using the ADIFDM to simulate chronoamperometric responses of an UME.

The ADIFDM has also been used to treat lateral proton diffusion studied by either SECMIT (Slevin and Unwin 2000) or a novel proton feedback method (Zhang and Unwin 2002a, 2002b). A more detailed description of the experimental configuration is given in section 6.1.2.3. These latter models take into account the potential-dependent association/dissociation constant of the interfacial acid groups, illustrating that SECM is sensitive to rather complex interfacial processes. A triple potential step method has been used to study the diffusion of redox-active amphiphiles in Langmuir monolayers at the water/air interface (description in section 6.1.2.2), and this has also been simulated using the ADIFDM approach in Zhang *et al* (2001).

The recent trend in SECM modelling has been towards the use of proprietary software packages, such as Comsol Multiphysics (previously Femlab; Comsol Ab, Sweden). Packages of this type provide several advantages over the direct implementation of numerical algorithms. Primarily, one is able to develop a model more rapidly, taking advantage of complex algorithms, which have been efficiently programmed. Graphical user interfaces (GUIs) have facilitated the input and modelling of complicated experimental geometries with relative ease, e.g. SECM–AFM probes (see section 2.3.4) (Dobson *et al* 2005, Holder *et al* 2005). Within the GUI, results of simulations are effectively visualized (figure 5). Also useful is the coupling of several equation systems covering different physical phenomena (Liljeroth *et al* 2002), e.g. hydrodynamics (Carlsson *et al* 2005), kinetics (Burt *et al* 2005a) and lateral charge propagation (O'Mullane *et al* 2004).

4. Basic SECM techniques and their applications

Several modes of SECM have been developed to allow the local chemical properties of interfaces to be investigated. A comprehensive review of SECM techniques covering up the period to the year 2000 can be found in the major edited volume on SECM (Bard and Mirkin 2001). Here we consider those methods that are most important in the study of biomolecular interfaces.

4.1. Tip detection methods

Local variations in concentrations above a target interface can be mapped with both potentiometric and amperometric probes. In this type of application, the detector probe is generally assumed to be passive (i.e. non-perturbing to the interfacial process).

Tip detection (or collection) measurements have proved particularly powerful for identifying localized transport pathways in synthetic membranes and biological tissues, e.g. dentine (Macpherson *et al* 1995a, 1995b, Unwin *et al* 1997, Macpherson and Unwin 2005) and

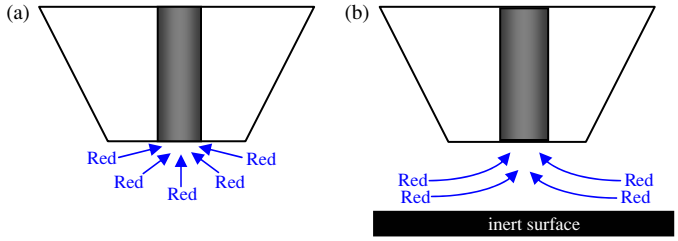

Figure 6. (a) Schematic of the hemispherical diffusion field established for the steady-state diffusion-limited oxidation of a bulk solution species, Red, at a disc-shaped UME, giving rise to a current $i(\infty)$. (b) When the UME is positioned close to an inert target interface, diffusion of Red from the bulk solution to the UME is hindered and the current, i, decreases.

mouse skin (White and Scott 1993). The tip detection approach is also useful for investigating the activity of immobilized enzymes. In this situation, the tip is used to detect the product as a result of electron transfer reactions exhibited by the immobilized enzyme under investigation. Systems studied include glucose oxidase (GOx) (Pierce *et al* 1992, Pierce and Bard 1993, Kranz *et al* 1997, Wittstock and Schuhmann 1997, Wijayawardhana *et al* 2000), urease (Horrocks *et al* 1993), horse radish peroxidase (HRP) (Shiku *et al* 1995, Zhou *et al* 1999), diaphorase (Shiku *et al* 1995, Yasukawa *et al* 2000a), nitrate reductase (Zaumseil *et al* 2000) and alkaline phosphatase (Wittstock *et al* 1995). Simple tip detection strategies are optimal when the surface kinetics are too slow to be measured by, for example, the feedback mode (see section 4.3.1). This is because the surface generation–tip collection has a negligible baseline signal and simply relies on the tip being sufficiently sensitive to detect the species of interest. However, mass transport between the tip and the surface, under tip detection conditions, may be complicated and ill defined, especially for complex surfaces, which show spatially heterogeneous reactivity.

As well as investigating enzyme activity, the tip collection technique has been used to map variations in concentration gradients near to living cells (see section 6.3).

4.2. Negative feedback mode

Many applications of SECM involve using the tip to locally perturb an interfacial process, by electrolysis or ion transfer, and determining the kinetic effect from the resulting tip current. In this situation, the tip is usually held at a potential to drive the detection of a target analyte (present in bulk solution) at a diffusion-limited rate (no electrode kinetic limitations to the current). The baseline response for these measurements, when the interface is inert with respect to the tip-detected species, is termed 'negative feedback' (Bard *et al* 1989, Kwak and Bard 1989b) and it is useful to consider this, by way of introduction to other modes, such as positive feedback (redox activity mapping) (section 4.3.1) and SECM-induced transfer (SECMIT) (section 4.3.2). When the tip is positioned at a relatively long distance from the target interface, $d > 10a$, where d is the tip–interface distance and a is the electrode radius, it behaves as a conventional UME. In this situation, a steady-state current, $i(\infty)$, is rapidly established due to hemispherical diffusion of the target species (Red in figure 6(a)). As the tip is brought close to an interface which is inert with respect to the species involved in the electrode process, diffusion to the UME is hindered (figure 6(b)) and the steady-state current, i, decreases compared to $i(\infty)$. In general, measurements of $i/i(\infty)$ as a function of d are termed 'approach curves'.

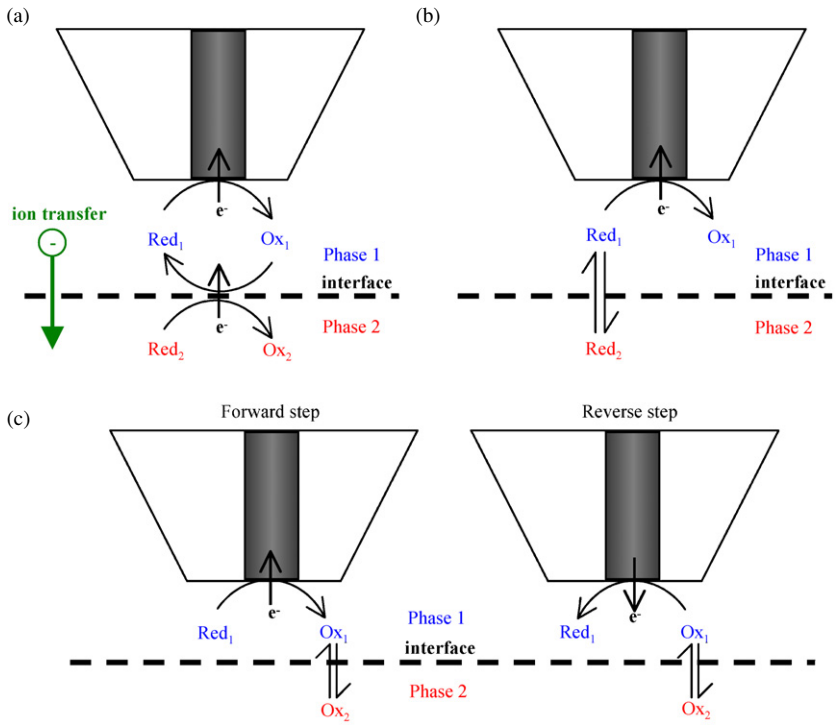

Figure 7. Principal methods for inducing and monitoring interfacial processes with SECM: (a) feedback mode; (b) induced transfer; (c) double potential step chronoamperometry.

Since the dependence of the $i/i(\infty)$ ratio on d and the tip geometry can be calculated theoretically (Kwak and Bard 1989b), using methodology such as that highlighted in section 3, simple current measurements with mediators which do not interact at the interface can be used to provide information on either the tip-to-sample separation or the topography of the sample of interest. For the latter application, an amperometric UME is typically scanned at a constant height above the target interface (x–y plane) and the diffusion-limited current for electrolysis of the target species is measured. This, in turn, can be related to the distance between the tip and the interface, from which topographical information is obtained.

When either the solution species of interest (Red in figure 6) or tip electrode reaction product(s) interact with the target interface, the hindered mass transport picture of figure 6(b) is modified. The effect is manifested in a change in the tip current, which is the basis of using SECM to investigate interfacial reactivity. Under these conditions, independent methods for determining topography of the sample are often useful.

4.3. Concept of using a SECM tip to perturb and monitor an interfacial process

There are three main ways in which an amperometric electrode has been used to both induce and monitor interfacial processes. The basic mass transport pictures in figure 7 serve to illustrate these methods, for the general cases where the liquid phase containing the UME is in contact with a second phase, which has fluid-like transport properties (e.g. a second immiscible liquid, biomaterial or gas). Although a redox reaction is considered at the tip, similar experiments

may be carried out with ion transfer voltammetric probes (described earlier in section 2.3.5). Transport processes in phase 2 can usually be neglected when phase 2 is a solid or a gas (due to the rapidity of gas transport compared to diffusion in liquids).

4.3.1. Positive feedback mode. The feedback mode, depicted in figure 7(a), is one of the most widely used SECM techniques, applicable mainly to the study of interfacial redox processes (Bard *et al* 1989), although feedback based on assisted ion transfer has also been reported (Shao and Mirkin 1997, 1998). For redox processes, the basic idea is to generate a species at the tip in its oxidized or reduced state (generation of Ox_1 in figure 7(a)), typically at a diffusion-controlled rate, by electrolysis of the other half of a redox couple (Red_1). The tip-generated species diffuses from the UME to the target interface. If it undergoes a redox reaction at the interface, which converts it to the original form, the mediator diffuses back to the tip, thereby establishing a feedback cycle and enhancing the current at the UME. The redox reaction could occur at a fixed site on the interface, as in the case of immobilized oxidoreductase enzymes (Pierce *et al* 1992, Pierce and Bard 1993, Kranz *et al* 1997). Alternatively, the reaction could require the diffusion of a partner species in phase 2 to the interface (Red_2 in figure 7(a)), as in the case of electron transfer at immiscible liquid/liquid interfaces.

Redox activity of individual metastatic and non-metastatic human breast cells has been investigated by SECM feedback experiments (Liu *et al* 2000). When highly charged hydrophilic mediators such as $Fe(CN)_6^{3/4-}$ and $Ru(NH_3)_6^{3/2+}$ were used, negative feedback behaviour was observed, indicating that these mediators did not permeate the cell membrane and undergo intracellular redox processes.

Schuhmann's group (Turcu *et al* 2004) has reported a straightforward electrochemical detection scheme based on the feedback mode which they have used for imaging microscopic spots of immobilized nucleic acids and allows recognition of DNA hybridization. In this work, oligonucleotides were spotted on conducting surfaces, which were then imaged using amperometric feedback mode SECM in electrolytes containing a negatively charged redox mediator ($[Fe(CN)_6]^{3-/4-}$).

Significant decreases in the positive feedback currents were observed above a DNA-modified region, which was attributed to electrostatic repulsion between deprotonated phosphate groups of the immobilized DNA and the charged redox mediator.

4.3.2. Permeability mapping–SECM-induced transfer (SECMIT). This technique, depicted schematically in figure 7(b), can be used to characterize reversible phase transfer processes at a wide variety of interfaces (Barker *et al* 1998). The basic idea is to perturb the process, initially at equilibrium, through local amperometry at the UME located in one of the phases, close to the interface with the second phase (Barker *et al* 1998, Evans *et al* 2000). A potential is applied to the tip, sufficient to deplete the species of interest in phase 1 (oxidation of Red_1 to Ox_1 in figure 7(b)), which drives the transfer of species Red from phase 2 to phase 1. This enhances the current, compared to the situation where there is no net transfer across the target interface and species Red reaches the tip only by hindered diffusion through phase 1. For a given tip–interface separation, the overall current response is governed by diffusion in the two phases and the interfacial kinetics (Barker *et al* 1998). This technique has mainly been used in conjunction with metal tips (Barker *et al* 1998), but ion transfer voltammetric probes can also be used (Evans *et al* 2000). SECMIT offers the advantage of non-invasive measurement of quantities in the second phase. It has proved particularly powerful in investigations of solute transfer across interfaces formed between biological tissues and a bathing solution (Macpherson *et al* 1997, Gonsalves *et al* 2000a, 2000b) where contact of UME with the

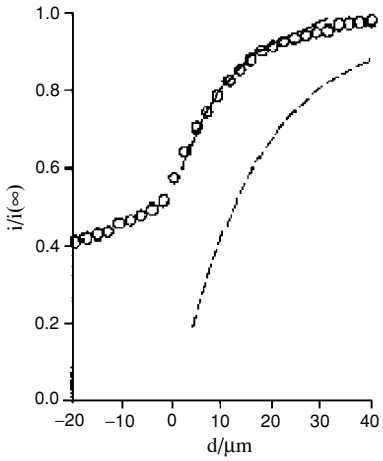

Figure 8. Approach curve of normalized steady-state current versus probe/interface separation for the diffusion-controlled reduction of oxygen at an UME scanned towards a sample of laryngeal cartilage (O). The dashed line shows the theoretical response for an inert interface (hindered diffusion only of oxygen in the aqueous phase containing the UME), while the solid line shows the behaviour for induced transfer with the oxygen diffusion coefficient having a value of 50% of that in aqueous solution. The partition coefficient for oxygen between the aqueous and cartilage phases was considered to be unity. (Reproduced with permission from Barker *et al* (1999), copyright 1999 Elsevier.)

sample itself might otherwise damage the sample or lead to contamination of the electrode surface. When there are no kinetic limitations to the interfacial transfer process, SECMIT is also an effective analytical technique for determining the permeability, concentration and diffusive properties of a solute in a target phase (Barker *et al* 1998).

SECMIT has been used successfully to measure the diffusion coefficient of oxygen in pig laryngeal cartilage. Figure 8 shows a typical steady-state approach curve for the diffusion-limited reduction of oxygen at a 25 μm diameter Pt disc electrode approaching a thin slice of cartilage in aerated aqueous electrolyte. Close to the interface, the measured currents are higher than predicted for an inert surface, since the electrolysis process promotes the transfer of oxygen from the cartilage matrix to the aqueous solution, enhancing the flux at the UME. Through these measurements, the space-averaged diffusion coefficient of oxygen in cartilage was estimated to be approximately 50% of that in aqueous solution (Macpherson *et al* 1997). It has also been established that the interterritorial regions, i.e. the areas between cells in the surface of the cartilage presented to the UME, provided the most facile transport pathways (Macpherson *et al* 1997).

4.4. Flow detection

Work from our group has used the imaging capabilities of SECM to quantify the rates of convective flow through tubules in dentine slices (Macpherson *et al* 1995a, 1995b, Unwin *et al* 1997, Macpherson and Unwin 2005), subjected to fluid pressures similar to *in vivo* pulpal pressures. Complementary studies (Nugues and Denuault 1996) examined diffusive transport through dentine slices. Fluid flow through exposed dentinal tubules in the tooth is important in the condition of hypersensitivity, and a fundamental understanding of fluid movement, at a local level, is needed to develop effective treatments. SECM studies demonstrated, for the first time, that convective rates across dentine varied dramatically at the local level (Macpherson

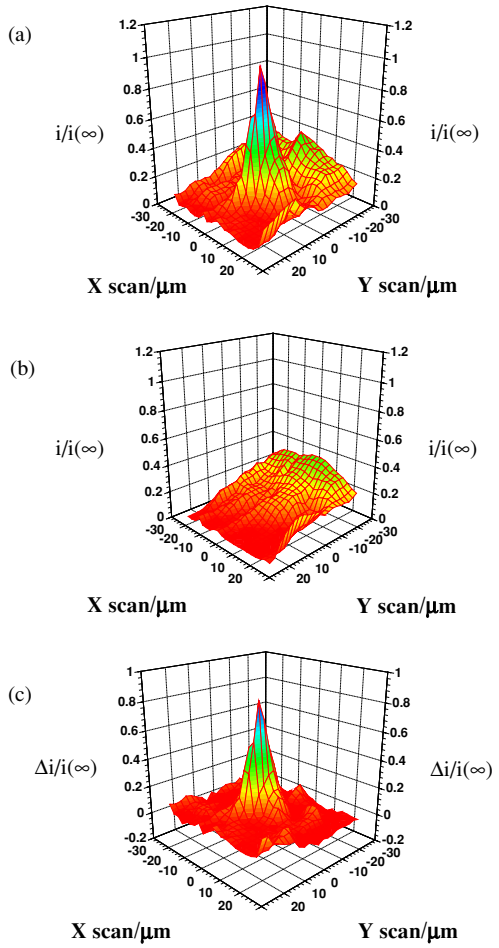

Figure 9. Images of the variation of normalized transport-limited current for the one-electron oxidation of ferrocyanide with a tip (1.0 μm radius) scanned in a plane parallel to a dentine surface. The data were obtained with (a) a pressure of 20 cm aqueous solution across a 50 μm thick dentine slice and (b) no solution pressure across the slice. The current difference image (c) highlights the areas of the sample through which localized mass transport occurs.

et al 1995a, 1995b, Unwin *et al* 1997). By using UMEs with small radii (down to 1 μm), it was possible to determine the rate of convection of an electrolyte solution containing ferrocyanide ions to the level of single tubules (2 μm diameter) (Macpherson *et al* 1995a). Figure 9 shows typical images of normalized transport-limited current for the one-electron oxidation of ferrocyanide as a function of tip position in the x–y plane parallel to a dentine surface. The data were obtained with (a) a hydrostatic pressure of 20 cm aqueous solution across a dentine slice and (b) in the absence of a pressure difference. In the latter case, the current was due solely to hindered diffusion of ferrocyanide, in the receptor phase containing the tip. By subtracting the image in figure 9(b) from that in figure 9(a), a difference plot of the normalized current, $\Delta i/i(\infty)$, figure 9(c), highlights clearly the regions of flow. For this particular case, flow was predominantly through one tubule, with several others showing limited activity. Since the 50 μm square area contained approximately 80 tubules, it was concluded that the

majority of tubules in this region showed no detectable flow, probably due to occlusions sub-surface. These results demonstrated that the localized flow rates in a single tubule may be significantly different from the mean flow rate obtained from bulk measurements averaged over the sample. Subsequent work investigated the effectiveness of blocking agents (Macpherson *et al* 1995b, Macpherson and Unwin 2005) in occluding tubules and retarding fluid flow.

5. Advanced tip positioning methods

As mentioned in section 2.2, in SECM the tip usually needs to be positioned close to an interface with high precision. Accurate positioning is achieved by attaching the tip to piezoelectric translators. However, this still leaves the problem of determining the exact separation of the tip electrode and the surface, which is a crucial piece of information in developing models alongside the experimental data. Generally, this problem is one of ascribing the point $d = 0$ or at least the 'distance of closest approach' of the electrode with the surface. Although one can use the amperometric response of the tip electrode in some instances (usually when a mediator can be employed which is inert with respect the surface of interest (Gonsalves *et al* 2000a, 2000b)), for many systems it may be difficult to add a redox-active species to the solution, without affecting the process of interest or the viability of the sample. Additionally, there may be challenges relating to low analyte concentrations or background processes (such as fouling of the electrode) in biological media which mean it is hard to measure the distance accurately from the amperometric response. Consequently, much effort has been directed towards the development of alternate procedures for tip positioning and distance determination, which are briefly considered in this section.

5.1. Shear force modulation

Control of the tip–substrate separation can be achieved by 'dithering' the electrode, via a small oscillation in the x–y plane. As the electrode is brought close to a surface, the oscillation is damped, to a degree which depends on the tip–substrate separation (Ludwig *et al* 1995). Images are usually acquired at constant damping amplitude, which corresponds to a constant distance between the tip and substrate; thus, the tip follows the surface contours. Perpendicularity of tip and surface is essential if the measured damping is to correspond to electrode position, and not merely that of the surrounding insulator. The oscillation amplitude is mainly monitored in one of the two ways, either (i) using a laser which is focused at the end of the tip electrode, with the signal detected by a split photodiode (Ludwig *et al* 1995, Hengstenberg *et al* 2000), or (ii) by monitoring the vibration amplitude of a tuning fork attached to the electrode (James *et al* 1998, Büchler *et al* 2000). The method of feedback described was originally used in near-field scanning optical microscopy (NSOM) (Betzig *et al* 1992).

With this experimental arrangement, it is possible to replace conventional SECM probes with an open glass capillary, opening up the possibility of filling the capillary with a myriad of 'chemical cocktails'. For example, in one study (Hengstenberg *et al* 2000) a glass capillary was filled with a biocatalyst, which could be released and detected at an underlying Pt electrode. Since the topographical resolution of this type of approach is determined by the diameter of the overall probe, the use of small, needle-type UMEs, such as those discussed in section 2.3.3, is essential for high-resolution electrochemical and topographical imaging (Ballesteros-Katemann and Schuhmann 2002). It is also important that the probe is of low mass to allow sufficient amplitude of oscillation.

5.2. Tip position modulation

Tip position modulation SECM refers to an operation where an amperometric tip is oscillated in a sinusoidal motion perpendicular to the surface (typical amplitude 10% of the tip radius). The resulting current varies with the frequency of the driving oscillation (Wipf and Bard 1992). The amplitude and phase of the oscillating current enable one to deconvolute the activity and topography of the surface (Wipf and Bard 1993). The phase of the current is the same as the phase of the tip–surface separation when the probe is oscillated above an inert surface, whereas they are entirely out of phase above a conducting surface (in positive feedback mode). It is expected that the amplitude of the oscillating current, for small amplitudes of oscillation, should be proportional to the derivative of the steady-state current, measured while the tip is held at the midpoint of its oscillation; equivalently, it is expected to be proportional to the derivative of the current–distance approach curve, again evaluated at the midpoint of the oscillation. This has been shown to be a good approximation for an active substrate (positive feedback mode); however, some small deviations from this are seen when the UME is allowed to approach an insulating surface (Wipf and Bard 1992). Furthermore, as the frequency of the current oscillation is known, low-frequency background noise (e.g. drift) is filtered out, meaning the signal is robust. A lock-in amplifier is generally used for this purpose.

5.3. SECM–AFM

SECM–AFM, as introduced in section 2.3.4, has the dual benefits of nanometre-resolution topographic imaging alongside the ability to electrochemically measure and/or perturb a system; these are mediated via the AFM probe and inbuilt electrode, respectively.

SECM–AFM has been used to image diffusion at microscale electrodes and transport through pores in membranes (Macpherson and Unwin 2000); several further studies have shown the approach suitable for single microscale and nanoscale pores (Macpherson *et al* 2002, Gardner *et al* 2005).

Figure 10 shows examples of SECM–AFM data. In (a), one can see the topography of an array of microelectrodes, while (b) shows the corresponding current map, which clearly indicates that one electrode is essentially inactive. These data were obtained with a microfabricated probe (Dobson *et al* 2005). In (c), a simple hand-made probe was used to image a synthetic membrane and (d) shows the corresponding current map. The combination of AFM and SECM in this case allows one to accurately characterize the topography of the pores and thus present a more thorough analysis of the transport phenomena which can be deduced from the magnitude of the current response (Gardner *et al* 2005). Thus far, SECM–AFM has only been applied to synthetic membranes, but there is no inherent reason for this restriction and biological applications should follow, with the more ready availability of probes.

SECM–AFM has also been used to simultaneously map enzyme activity, as seen in section 4.1, and topography. Glucose oxidase (GOD) activity has been mapped, both while supported in a soft polymer matrix, electrodeposited on a micropatterned substrate (Keung *et al* 2003), and through a synthetic membrane (Keung *et al* 2005). The technique has also been used to image immobilized horseradish peroxidase (Kranz *et al* 2004).

SECM–AFM also has the potential to perturb interfacial systems through electrochemistry, while simultaneously imaging topography. Hitherto, this methodology has been applied to crystal dissolution studies (Jones *et al* 2003), but it is clear that future measurements could be performed on a wide variety of biophysical systems.

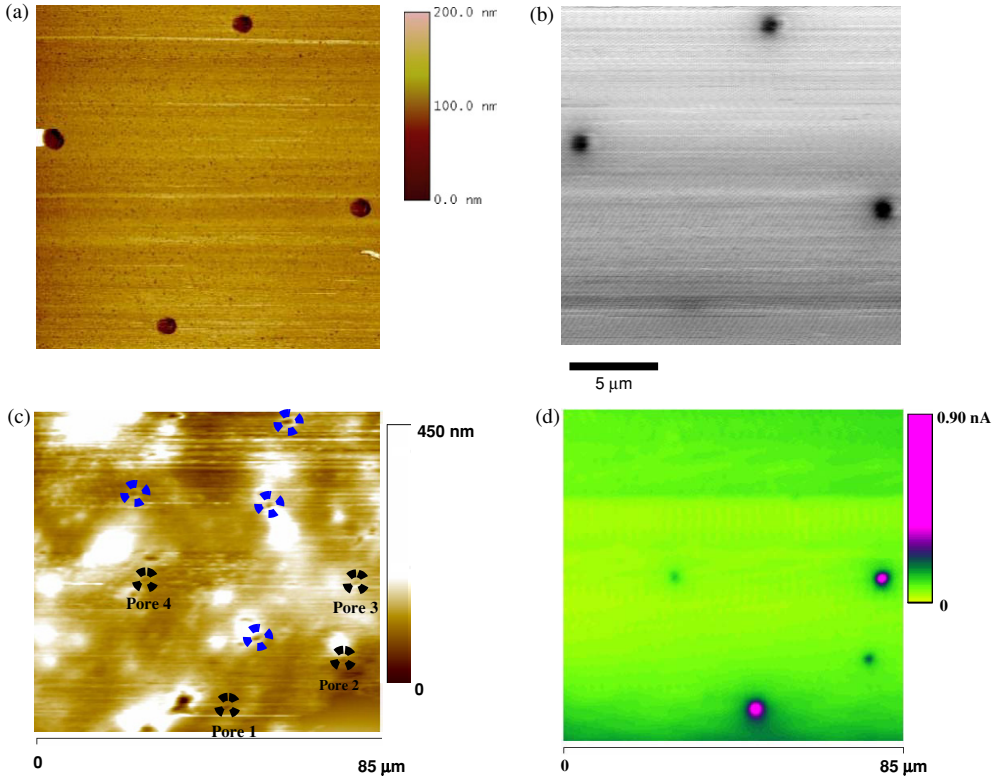

Figure 10. (a) Topography and (b) unfiltered fixed-height current maps for the diffusion-controlled tip detection of $Ru(NH_3)_6^{2+}$, generated from the diffusion-limited reduction of $Ru(NH_3)_6^{3+}$ at an array of 1 μm diameter substrate electrodes. SECM–AFM topography (c) and fixed-height current images (d), illustrating the structure and transport activity of a synthetic membrane. The SECM–AFM probe, placed in the receptor phase, was biased at a potential sufficient to detect $Fe(CN)_6^{4-}$ at a transport-controlled rate. The blue circles in (c) highlight some of the potential candidates for open pores (not all are ringed). The black circles show the pores which are active to transport. (Reprinted with permission from Dobson *et al* (2005) (a and b), copyright 2005 American Chemical Society, and Gardner *et al* (2005) (c and d), copyright 2005 Elsevier.)

6. Exotic interfaces

6.1. Monolayer studies

As illustrated in figure 11(b), one half of a bilayer membrane, a monolayer, constitutes a useful model system for investigating physicochemical processes pertinent to cellular membranes (Gennis 1989, Möhwald 1995). SECM has found successful application in the study of physicochemical processes at liquid interfaces modified with monolayers (Bard *et al* 1995, Barker *et al* 2001). Much of this work has considered the kinetics of molecular, ion and electron transfer processes, with the monolayer formed at a liquid/liquid interface (Strutwolf *et al* 2001, Zhang and Unwin 2002d, Zhang *et al* 2003, Cannan *et al* 2004), but the transfer of small molecules across the water/gas interface has also received attention (Slevin *et al* 1998, Zhang and Unwin 2002c, 2003, Borden and Longo 2004, Pu *et al* 2005).

6.1.1. Monolayers at liquid/liquid interfaces. Monolayers at oil/water interfaces constitute an attractive and simple model for a biomolecular interface, since the potential drop across the

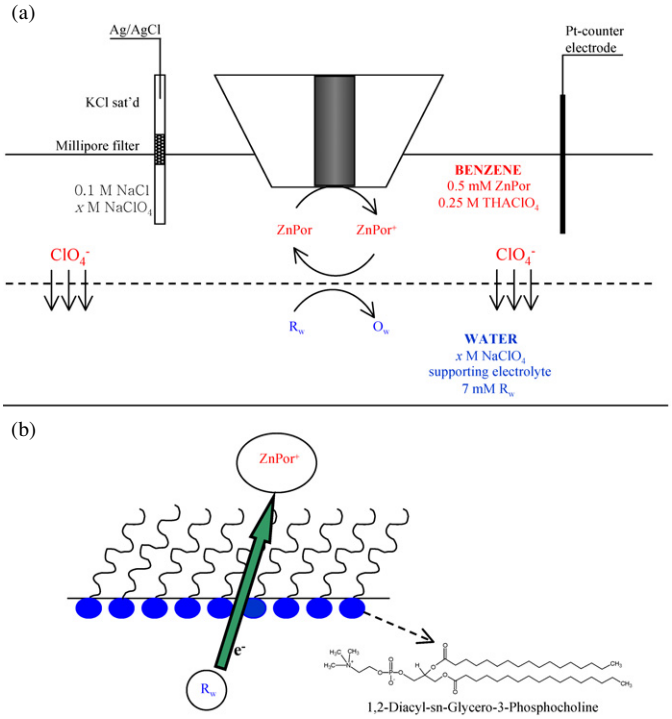

Figure 11. (a) Probing the kinetics of electron transfer (ET) between $ZnPor^{+}$ and various aqueous redox species at a liquid/liquid interface with the SECM feedback mode. O_w/R_w is an aqueous redox couple, such as $Ru(CN)_6^{3/4-}$, $Mo(CN)_8^{3/4-}$, $Fe(CN)_6^{3/4-}$, $Fe^{3+/2+}$, $V^{3+/2+}$ or Co(III)/(II) sepulchrate. Of the ionic species contained in the system, only ClO_4^- can readily cross the interface to maintain electroneutrality. (b) ET across a liquid/liquid interface modified by a monolayer of phospholipid. The inset shows the structure of a synthetic phosphatidylcholine lipid used in the studies described in the text.

interface can readily be controlled and varied, thereby allowing the effect on charge transfer kinetics to be identified (Girault and Schiffrin 1989, Volkov *et al* 1998).

Distance effects on electron transfer between redox species confined to two separate phases have been investigated using SECM, with variable chain length phospholipid monolayers adsorbed at the liquid/liquid interface serving to separate the reactants in the two immiscible phases (Tsionsky *et al* 1997a); see figure 11. These investigations involved the reaction between tip-generated 5,10,15,20-tetraphenyl-21*H*,23*H*-porphine zinc cation ($ZnPor^{+\cdot}$) in a benzene phase and various aqueous phase reductants (R_w in figure 11). The electron transfer rate constants, measured in the presence of the phospholipid monolayer, were lower than for the lipid-free interface and generally decreased as the number of methylene groups in the hydrocarbon chain of the phospholipid increased. Some deviations from this trend were observed, that were attributed to the partial penetration of the $ZnPor^{+\cdot}$ species into the lipid monolayer.

In a separate study (Delville *et al* 1998), the rate of electron transfer across an oil/water interface in the presence of adsorbed conjugated phospholipids was found to be at least twice that measured when saturated phospholipids were used. This effect was interpreted in terms of the delocalized conjugated chain acting as a conductive wire, so increasing the rate of electron transfer between the redox species in the two phases. The difference in electron transfer rates

with saturated and conjugated phospholipids was sufficiently high to enable the use of the SECM feedback mode to image electron transfer rates across mixed monolayers (Delville *et al* 1998). When a 25 μm diameter disc UME generating $ZnPor^{+\cdot}$ in benzene was scanned laterally across a mixed monolayer, regions of relatively high and low ET rates were detected from changes in the SECM feedback current due to the reaction with reductants in the aqueous phase. These zones had dimensions of tens of microns and were considered to be associated with domains that were rich in one of the lipid types. The effect of temperature on interfacial electron transfer rates for saturated phospholipids has also been investigated (Delville *et al* 1998). A sharp decrease in the rate constant at a critical temperature was attributed to a phase transition changing the tunnelling distance between the redox species contained in the two contacting solutions.

6.1.2. Monolayers at water/air (W/A) interfaces. A wide range of diffusion processes can be investigated in molecular monolayers at the W/A interface, by combining SECM with a Langmuir trough. The use of a Langmuir trough enables the effect of monolayer compression on the process of interest to be readily investigated.

6.1.2.1. Transfer of neutral molecules across Langmuir monolayers at a W/A interface. The transfer of oxygen across a W/A interface in the absence and presence of a monolayer of 1-octadecanol has been investigated with SECM (Slevin *et al* 1998). This study provided information on the effect of the monolayer on re-aeration rates, which is of importance in natural environments (Schwarzenbach *et al* 1993, Thibodeaux 1996, Donaldson and Vaida 2006).

For these investigations, the submarine UME was deployed in an aqueous sub-phase, which contained 0.1 M KNO_3, and held at a potential to reduce oxygen at a diffusion-controlled rate. With the probe positioned close to the W/A interface, the electrochemical process promoted the transfer of O_2 from air (phase 2) to the aqueous solution (phase 1), with subsequent collection of O_2 at the UME; figure 12. Given the high diffusion coefficient and concentration of oxygen in the air phase, depletion effects in phase 2 were unimportant and this simplified the modelling of the process. The results of the study demonstrated that the rate of oxygen transfer across a clean W/A interface was diffusion controlled on the time scale of SECM measurements (the characteristic time scale $t \sim \frac{d^2}{D}$, where d is the tip interface distance and D is the diffusion coefficient in the aqueous phase). The rate of this transfer process was, however, significantly reduced with increasing compression of a 1-octadecanol monolayer assembled at the W/A interface. Approach curves for oxygen reduction were recorded for the monolayer at different surface pressures. In these studies, it was found that the molecular area at which the monolayer collapsed corresponded to a state where oxygen transfer was significantly inhibited.

This approach was further extended to include monolayers of lipids, 1-octadecanol and an investigation of the deformation of the liquid/air interface by the probe (Ciani *et al* 2004). The rate constant for oxygen transfer across the W/A interface, K_{wa}, decreases with increasing surface pressure for 1-octadecanol (abbreviated as $C_{18}OH$ below) and L-α-dipalmitoyl phosphatidic acid (DPPA) monolayers using a hemispherical mercury microelectrode as a SECM probe. As illustrated in figure 13, the increase in surface pressure of the monolayers was accompanied by a decrease in O_2 transfer across the interface, evident by the decrease in current for O_2 reduction at any normalized tip–interface distance, d/a.

To further examine the effect of permeant size and amphiphile chain length on molecular transfer, the diffusion of Br_2 across a W/A interface modified with different chain length fatty

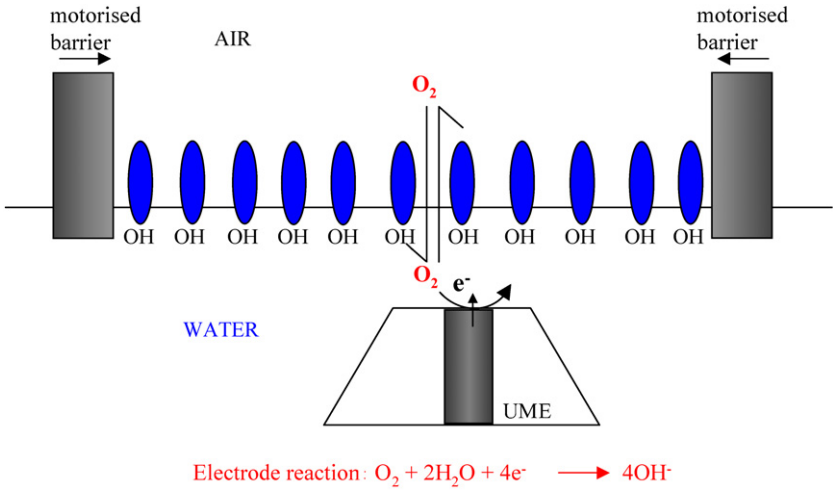

Figure 12. Schematic illustration (not to scale) of the SECM-induced transfer of oxygen across a 1-octadecanol monolayer at the air/water interface.

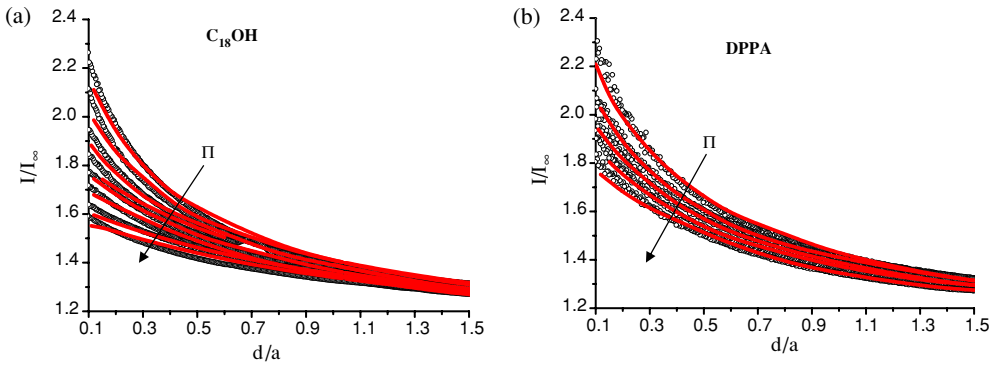

Figure 13. Normalized experimental approach curves for oxygen reduction at a hemispherical microelectrode approaching a W/A interface for various (a) $C_{18}OH$ and (b) DPPA monolayer pressures. From top to bottom, the curves correspond to uncompressed and surface pressures of 5, 10, 15, 20, 25, 30 and 40 mN m^{-1} in (a) and 5, 10, 20 and 30 mN m^{-1} in (b). The solid lines represent the theoretical behaviour for k_{wa} (cm s^{-1}).

alcohols was considered (Zhang and Unwin 2002c). A homologous series of aliphatic 1-substituted alcohols was investigated: $C_{14}H_{29}OH$, $C_{16}H_{33}OH$, $C_{18}H_{37}OH$, $C_{20}H_{41}OH$. Kinetic data were interpreted in terms of different theories: the accessible area model (Barnes *et al* 1970), the energy barrier model (Langmuir and Langmuir 1927, Langmuir and Schaefer 1943, Barnes and La Mer 1962), the density fluctuation model (Blank 1964, Blank and Britten 1968) and the solubility–diffusion model (Gennis 1989).

The principles of these experimental measurements, which employed the SECM–DPSC mode, are illustrated in figure 14. Br_2 was electrogenerated in an initial (forward) potential step by the diffusion-controlled oxidation of Br^- in an aqueous sulfuric acid sub-phase. Tip-generated Br_2 diffused to and transferred across the fatty alcohol monolayer irreversibly. Br_2 was subsequently collected back by diffusion-controlled reduction to Br^- in a second (reverse)

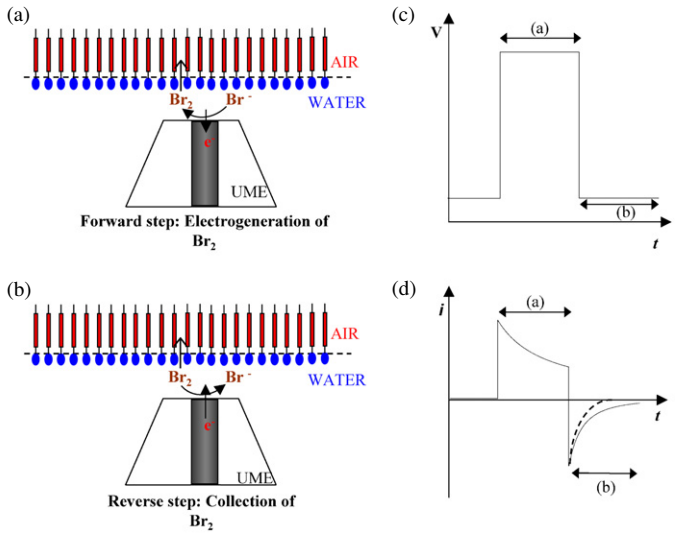

Figure 14. Schematic (not to scale) of SECM–DPSC measurements. Molecular Br_2 is generated by oxidizing Br^- in the forward potential step (a) and collected when the direction of the potential step is reversed to reduce Br_2 to Br^- (b). Schematic representations of the current (c) (with (– – –) and without (——) Br_2 transfer across the interface) and potential (d) responses are illustrated with respect to time, for the forward (a) and reverse (b) steps.

potential step. The resulting current–time behaviour provided information on both the tip–interface separation (forward step) and the kinetics of Br_2 transfer (reverse step) (Slevin *et al* 1997).

6.1.2.2. Lateral amphiphile diffusion. A SECM approach for studying the lateral diffusion of redox-active amphiphiles in Langmuir monolayers at a W/A interface has been developed (Zhang *et al* 2001). Analogous to fluorescence recovery after photobleaching (FRAP) (Edidin 1981, Peters 1981, Vaz *et al* 1982, Elson 1985, 1986), the electrochemical approach involves an 'electrochemical bleaching' step, a 'recovery' step and a final 'analysis' step, as illustrated schematically in figure 15. Practically, a triple potential step is applied at a submarine UME placed in the aqueous sub-phase of the Langmuir trough, close (1–2 μm) to the monolayer. In the first potential step, an electroactive species is generated at the UME by diffusion-controlled electrolysis of a precursor. This species diffuses to, and reacts with, the redox-active amphiphile at the W/A interface resulting in the formation of the initial solution precursor, which undergoes diffusional feedback to the UME. In this first step, the rate constant for electron transfer between the solution mediator and the surface-confined species can be measured from the UME current–time transient. In the second period, the potential step is reversed to convert the electrogenerated species to its initial form. Lateral diffusion of electroactive amphiphile into the interfacial zone probed by the UME occurs simultaneously in this recovery period. In the third step, the potential is stepped in the same direction as for the first step. The corresponding UME current–time transient can be used to determine either the distance between the UME tip and the monolayer at the water surface (if an extensive first step and a short second step are utilized), or the lateral diffusion coefficient of the amphiphile (if a longer recovery period is set).

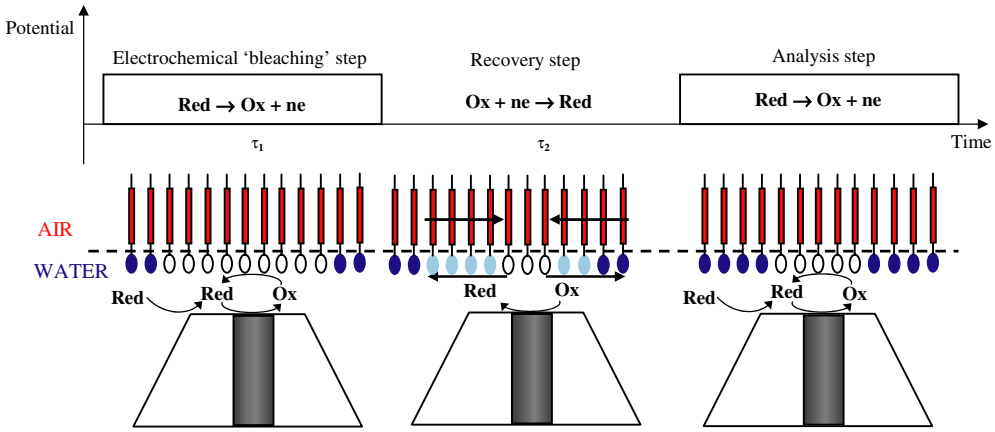

Figure 15. Schematic (not to scale) of the arrangement for SECM triple potential step measurements of lateral diffusion processes at the W/A interface.

This method was demonstrated experimentally with measurements on the lateral diffusion of *N*-octadecylferrocenecarboxamide in a 1:1 Langmuir monolayer with 1-octadecanol (Zhang *et al* 2001). There are prospects for applying this type of approach to redox reactions in biologically relevant assemblies. This, and related, methods have also been used to study lateral charge transfer in ultrathin polymer films (Mandler and Unwin 2003, O'Mullane *et al* 2004).

6.1.2.3. Lateral proton hopping along monolayers. An approach similar to SECMIT has been used to investigate lateral proton diffusion processes in acidic monolayers (Slevin and Unwin 2000). Lateral diffusion processes of this type are crucial in defining the activity of membrane-bound reactive centres in cells (Teissié *et al* 1993). A controversial aspect of prior work has been the magnitude of the lateral proton diffusion coefficient, since different techniques have provided contradictory results (Teissié *et al* 1985, 1993, Prats *et al* 1986, Nachliel and Gutman 1988, Gabriel and Teissié 1991, 1996, Gutman and Nachliel 1995, Leite *et al* 1998). Many of the earlier measurements were made over centimetre length scales (Teissié *et al* 1985, 1993, Prats *et al* 1986, Gabriel and Teissié 1991, 1996, Leite *et al* 1998); a key advantage of SECM is the ability to make measurements with high spatial and temporal resolution, pertinent to cellular membranes.

SECM was initially used to investigate lateral proton diffusion at stearic acid (Slevin and Unwin 2000) assembled at the W/A interface on an aqueous sub-phase containing a low concentration of protons (20–50 μM). The UME was biased at a potential suitable to reduce protons to hydrogen at a diffusion-controlled rate. The resulting local depletion drove the interfacial acid dissociation reaction, which in turn created a proton diffusion gradient, both in solution and at the interface (figure 16).

The transport-limited current flowing at the electrode provided a measure of the rates of the solution and surface processes, which were investigated as a function of the surface coverage of stearic acid, by controlling the monolayer compression. It was found that the surface-pressure dependent surface diffusion coefficient was a fraction of that in solution.

A SECM proton feedback method has been developed for investigating lateral proton diffusion at phospholipid assemblies, specifically Langmuir monolayers at the W/A interface

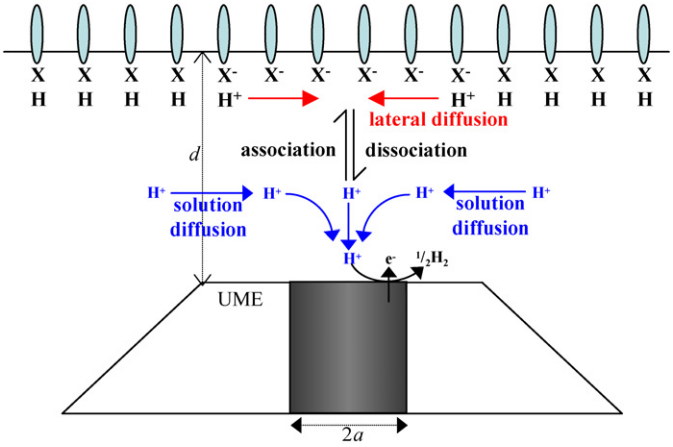

Figure 16. Schematic (not to scale) of the arrangement for SECM measurements of proton transport at a stearic acid monolayer deposited at the W/A interface. The UME typically had a diameter, $2a$, in the range 10–25 μm and the tip–interface distance, d, was typically $\leqslant 2a$.

(Zhang and Unwin 2002c). In this approach, a base is electrogenerated by the reduction of a weak acid at a submarine UME placed in the aqueous sub-phase of a Langmuir trough close to a monolayer. The base diffuses to the interface and titrates monolayer-bound protons and is thus converted back to the acid form, so enhancing the current response at the UME. Lateral proton diffusion has been investigated in monolayers comprising either acidic DL-α-phosphatidyl-L-serine, dipalmitoyl or zwitterionic L-α-phosphatidylcholine, dipalmitoyl monolayers at a range of surface pressures (Zhang and Unwin 2002c). In the former case, the surface diffusion coefficient was again found to be a fraction of that in bulk solution.

6.2. Bilayer studies

The properties of bilayer lipid membranes (BLMs) are of great interest, as BLMs are considered to be reasonable artificial analogues for cellular membranes (Tien 1974). Transport processes at cell membranes are of vital biological importance, and artificially constructed BLMs can be modified to mimic selected properties of living membranes (Tien 1974).

BLMs can readily be prepared in a form suitable for study by a variety of techniques, including SECM. For example, phospholipid solutions in decane can simply be 'painted' across an aperture in a supporting sheet (usually Teflon^{TM}) positioned in an aqueous solution and allowed to thin out to form a bilayer (Mueller *et al* 1963). Alternatively, BLMs can be formed via a 'monolayer folding' technique from thin films spread at the W/A interface (Montal and Mueller 1972). The latter method has the advantage that it can be used to produce bilayers composed of two different monolayers. Moreover, this technique minimizes solvent inclusion effects that may result from painting techniques. BLMs can be modified to mimic a specific property of a cell membrane; they are often more robust than living cells and may be made on a larger scale for physicochemical studies.

BLMs have been studied extensively since the 1960s, with electrical (impedance and capacitance) methods proving popular for characterizing the thickness and successful formation of a bilayer (Hanai *et al* 1964). Other early studies included an examination of the change in the electrical properties of bilayer membranes with the addition of salts (Tien

and Diana 1967). The advent of SECM and related microelectrode techniques has further advanced the study of BLMs and their properties at the local level, as considered in the following sections.

6.2.1. Topographical imaging of BLMs using SECM. Bard and co-workers have imaged the topography of BLMs (Tsionsky *et al* 1999). Membranes were prepared using the paintbrush technique and the cell design ensured equal pressure on either side of the membrane, resulting in the formation of a stable BLM. To image the bilayer topographically, the SECM probe was held at a potential suitable for the diffusion-limited oxidation of ferrocyanide, which was employed as the mediator in aqueous solution. Unmodified BLMs are inert to the transport of the highly charged ferrocyanide complex and so as the UME probe approached the bilayer, the current decreased as diffusion to the electrode became more hindered, following the negative feedback response (Kwak and Bard 1989b). In these studies, the probe electrode was moved perpendicularly towards the bilayer until the current was approximately 80% of that in bulk solution. It was then scanned, at a fixed height, from one side of the bilayer to the other. The current changes recorded could be related to a change in the tip–membrane separation, using the simple relationship between tip current and tip–surface distance (Kwak and Bard 1989b), thereby revealing the topography of the membrane. Results from these studies showed a structure in which a large central area consisted of a planar bilayer, surrounded by a torus of solvent and lipid which accumulated at the edges of the aperture.

6.2.2. SECM and microelectrode studies of charge transfer across BLMs. Matsue and co-workers were the first to use linear sweep voltammetry at UMEs to examine the permeation of ions through a BLM (Yamada *et al* 1991). Specifically, $Ru(NH_3)_6^{3+}$ and ferrocenecarboxylic acid (FCA) were used as target ions. A two-electrode system was used, with a 65 μm diameter Pt disc-shaped working electrode and an Ag/AgCl reference electrode. Both electrodes were immersed in solution on the same side of the BLM, with the working electrode held in close proximity to the membrane and attached to a motor-driven positioning stage.

The solution on both sides of the membrane had the same composition. A series of voltammograms were recorded at different electrode–bilayer distances and the change in the magnitudes of the limiting currents for the reduction of $Ru(NH_3)_6^{3+}$ and the oxidation of ferrocenecarboxylic acid (FCA) was monitored.

As the electrode–BLM distance decreased, there was a marked diminution in current for $Ru(NH_3)_6^{3+}$, leading to the conclusion that the BLM was practically impermeable to $Ru(NH_3)_6^{3+}$ transport. This allowed data obtained from the $Ru(NH_3)_6^{3+}$ experiments to be used as a measure of the tip–substrate distance, as might be done in the analysis of a SECM hindered diffusion curve (Kwak and Bard 1989b). On the other hand, FCA was found to transfer across the BLM.

Matsue and co-workers made further SECM studies of the transport properties of a BLM containing ion channels formed from alamethicin (Matsue *et al* 1994), which is selective to cations. The permeation of $Ru(NH_3)_6^{3+}$, $Fe(CN)_6^{3-}$ and I^- through the ion channels in the BLM was investigated and reported. Using a four-electrode system, a schematic of which is shown in figure 17, potentials were applied across the membrane, to facilitate opening of the channels which occurred at a membrane potential of 50 mV. The number of alamethicin molecules forming an average channel was determined by monitoring the dependence of the total ionic current on alamethicin concentration.

In order to monitor permeation, a voltage pulse was applied to the membrane and the reduction current was recorded for the detection of $Ru(NH_3)_6^{3+}$ by amperometry at a Pt UME

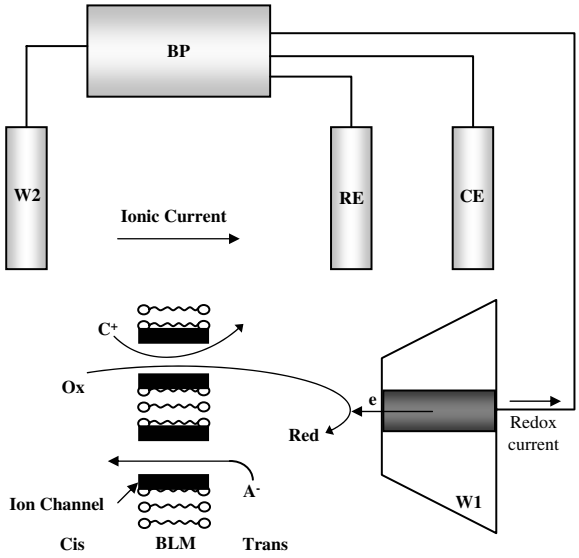

Figure 17. Schematic of the apparatus used to make simultaneous ionic and redox current measurements of transport across a BLM. BP = bipotentiostat; W1 = Pt microdisc electrode; W2 = Ag/AgCl electrode; RE = Ag/AgCl connected to virtual ground; CE = Pt wire.

held at selected distances from the *trans* side of the membrane. These data were used to calculate the relative permselectivity, P_R, of the redox ion compared to that of K^+. For $Ru(NH_3)_6^{3+}$, P_R was determined to be 0.27.

By reversing the potential across the membrane, it was possible to obtain, by the same method, relative permeabilities for $Fe(CN)_6^{3-}$ and I^-. The relative permeability of $Fe(CN)_6^{3-}$ was found to be much lower than for $Ru(NH_3)_6^{3+}$, which was attributed to electrostatic repulsion effects between $Fe(CN)_6^{3-}$ and the carbonyl groups on the walls of the ion channel. This was consistent with previous findings, showing that the weakly cation-selective alamethicin channels (Menestrina *et al* 1986) resisted the permeation of multi-charged negative ions.

Bard and co-workers also investigated the transport of I^- across BLMs using SECM approach curves (Tsionsky *et al* 1999). It was found that the flux of I^- to the electrode tip was considerably enhanced by the addition of I_2 to the membrane forming solution, suggesting that this acted as a carrier for I^- transport, via the formation of I_3^-.

6.2.3. Permeation of uncharged solutes across BLMs. SECM has been employed to examine the permeation of oxygen through BLMs formed from L-α-phosphatidylcholine (Gardner and Unwin 2000). Initially, the bilayer was approached with an UME held at a suitable potential for the diffusion-limited oxidation of $IrCl_6^{3-}$ (added to the solution). As the BLM was inert towards this ion, the resulting approach curves provided information on the tip–bilayer distances. The tip was then retracted and the potential changed to one suitable for the reduction of oxygen (naturally present in the aerated solution). In this case, the BLM was permeable to the transport of oxygen, the current remained similar to that obtained in bulk solution throughout the current–distance approach curve, due to the transport of O_2 across the BLM, with no apparent interfacial resistance.

An advantage of SECM in this application is that the tip induces the transport process and so there are no significant stagnant layers of the type involved in conventional transport

measurements, so allowing much faster interfacial processes to be characterized. These stagnant or 'unstirred' layers can, in fact, be probed using microelectrodes, as discussed in the following section.

6.2.4. Factors influencing membrane transport processes. Pohl and co-workers undertook a series of electrochemical studies, employing UMEs, to investigate BLM transport processes. For these studies, the physical environment of the bilayer and/or the mechanism of the transport process were of interest, as well as the properties of the unstirred 'diffusion layer'. This latter work extended existing biological and physiological models to provide a more 'realistic' interpretation of processes occurring in unstirred layers. For example, studies were carried out to measure the concentration profiles in the immediate vicinity of a BLM, i.e. across the unstirred layer and the effect of a transmembrane osmotic flux was measured (Pedley 1980, Pohl *et al* 1997).

The importance of the presence of unstirred layers has been cited in biological and physiological systems (Finkelstein 1976, 1987, Läuger 1976). For example, the existence of an unstirred layer around the erythrocyte cell membrane is believed to slow the O_2 uptake in man by a factor of at least 1.8–2.0 (Holland *et al* 1985) and the diffusion of cholesterol molecules through an extracellular unstirred layer influences cholesterol efflux from cell membranes (Rothblat *et al* 1992).

It has been shown that microelectrodes could be used to monitor and resolve the effects of the competing processes of ion and water fluxes across BLMs (Finkelstein 1987, Pohl *et al* 1998a, Pohl and Saparov 2000). From the concentration profile and membrane potential difference data, it was possible to determine the hydraulic membrane permeability, the single-pore water permeability coefficient and the number of water molecules transferred per ion (Pohl and Saparov 2000). This methodology has been used by Pohl and co-workers (Pohl *et al* 1997, 1998b) to examine related aspects of membrane transport.

6.3. Cellular processes

Chemical analysis of individual cells is important. Biological systems are rarely composed of populations of homogeneous cells, but are organized into spatially heterogeneous groups (such as organs), with individuals within the group often possessing very different activities. Cell heterogeneity has been difficult to assess by traditional biochemical approaches, especially when attempting to simultaneously correlate spatial distribution and altered cellular activity. SECM has the potential both to provide topographic information and to assess cellular functions such as photosynthesis, respiration and membrane transport, providing new insights into cellular heterogeneity. The following discussion is divided into sections based on the biological systems under investigation. Interested readers are referred to recent reviews of SECM in single-cell studies (Yasukawa *et al* 2000b, Horrocks and Wittstock 2000, Bard *et al* 2006, Amemiya *et al* 2006).

6.3.1. Photosynthesis. In one of the first applications, the surfaces of intact leaves of a grass, *Ligustrum sinensis*, were imaged using ferricyanide as a mediator and the negative feedback mode (Lee *et al* 1990). The images obtained were able to resolve the venation characteristics of the leaves and individual open stomata structures. Oxygen production upon illumination was also detected using the tip detection mode for a water plant, Elodea. A similar approach has been applied to image and monitor the photosynthetic activity of individual guard cells within the stomata of the variegated leaves of *Tradescantia fluminensis* (Tsionsky *et al* 1997b) *in vivo* from an intact plant. The topography of the leaves was obtained in the dark by

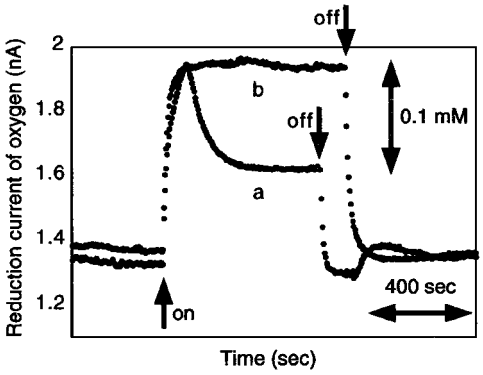

Figure 18. Responses of oxygen reduction current upon light irradiation (25 kLx) without (a) and with (b) 1.00 mM benzoquinone (BQ) in solution. A carbon microelectrode was placed approximately 1 μm away from a protoplast membrane. The reduction current for the oxygen was measured by differential pulse amperometry (DPA, 0.10 $\rightarrow$ -0.60 $\rightarrow$ -0.90 V versus Ag/AgCl, 0.50 $\rightarrow$ 3.00 $\rightarrow$ 0.50 s). The generation oxygen rate in the presence of 1.00 mM BQ is large compared with that without BQ. BQ functions efficiently as an electron acceptor to accelerate the photosynthetic electron transfer to increase the oxygen generation. (Reproduced with permission from Yasukawa *et al* (1999b), copyright 1999 Biophysical Society.)

using the negative feedback mode with oxygen as a mediator. SECM approach curves for oxygen reduction were measured for a tip positioned above an individual open guard cell in the dark and upon illumination. In addition, the response to step changes in light intensity was obtained for different regions of the leaf with varying photosynthetic activity, in the green (chloroplasts present in mesophyll and guard cells) and white areas (chloroplasts present in guard cells only). In the latter case, the tip current for oxygen evolution was of the order of pA, indicating that SECM is a sufficiently sensitive technique to detect the small flux of oxygen evolved from individual guard cells. More recently, SECM has been used to measure the *in vivo* photosynthetic activity of individual stomatal cells of *Brassica juncea* in response to cadmium-induced stress (Zhu *et al* 2005). This plant can accumulate heavy metals from the environment and so has use in bioremediation of contaminated soils; however, the heavy metals have a detrimental effect on photosynthesis rate and stomata physiology. High-resolution images of the lower surface of a leaf indicated that the stomatal density and size of the pore aperture were reduced, whereas the overall size of the stomatal complex increased in the Cd^{2+}-treated plants. The flux of oxygen through the stomata was also reduced in the Cd^{2+}-treated plants.

Photosynthetic oxygen evolution by single protoplasts from the marine alga *Bryopsis plumosa* (radius $\sim$100 μm) has also been monitored by measuring the oxygen reduction current at an UME positioned near to the cell surface (Yasukawa *et al* 1999a, 1999b, 2000b). In the dark, the cell consumed oxygen by respiration, whereas upon illumination net oxygen generation was observed, which increased to a peak shortly after the onset of illumination before declining to a lower steady-state value (figure 18). This decline was attributed to the dependence on the generation of photosynthesis substrates such as $NADP^+$ and ADP. SECM images showed a decline in the photosynthetic activity of the protoplast following injection of 3-(3,4-dichlorophenyl)-1,1-dimethylurea (DCMU), which is a known inhibitor of electron transfer in the photosynthetic chain. Figure 19 shows curves of the tip current for the localized oxygen concentration (derived from the tip current measured at a 1.1 μm Pt disc-shaped UME) as a function of distance from the chloroplast surface at different light intensities (Yasukawa

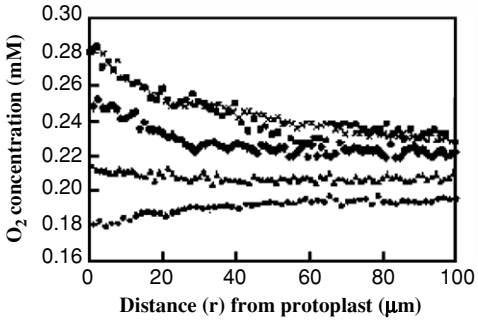

Figure 19. Variation of oxygen concentration as a function of the UME–protoplast (centre) distance under light irradiation with different intensity. Probe: Pt UME (radius 1.1 μm). Radius of the protoplast: 50 μm; light intensity: (■) 25 kLx, (×) 15 kLx, (♦) 10 kLx, (▲) 5 kLx, (●) 0 kLx (Lx = lumen m^{-2}). (Reproduced with permission from Yasukawa *et al* (2000b), copyright 2000 Wiley.)

et al 2000b). It can be seen that as the light intensity increases, the concentration of O_2 increases concomitantly. Dual SECM topography and photosynthetic oxygen generation images of a single living protoplast (Yasukawa *et al* 1999a) have been acquired simultaneously by using an individually addressable double ultramicroelectrode as the probe. In this application, one Pt disc electrode was used to detect an impermeable mediator, ferrocyanide, by oxidation and hence provide a topographical image, whereas the other disc electrode served to detect oxygen.

The effect of benzoquinone (BQ), which can permeate the cell membrane and accept electrons from the photosynthetic electron transport chain, has also been investigated, by measuring the reduction of benzoquinone and the generation of hydroquinone (Yasukawa *et al* 1999b). The addition of the inhibitor, DCMU, dramatically reduced the response, indicating that BQ accepts electrons from the electron transfer chain after the photosystem II site. Production of oxygen in the light was enhanced in the presence of benzoquinone and showed no peak in the response immediately following illumination, but rose to a steady-state level (figure 18).

6.3.2. Respiration. Respiration of several cell types has been studied using the SECM by amperometrically probing the concentration gradient of oxygen or a redox species capable of participating in the electron transport chain, such as ferro/ferricyanide, near to the cell surface (Kaya *et al* 2003, 2004, Torisawa *et al* 2003, Holt and Bard 2005).

The respiratory activity of individual cultivated cancer cells has been investigated (Yasukawa *et al* 1998, Kaya *et al* 2003) and areas of low oxygen were observed which coincided with the location of the living cells. Following exposure to KCN, respiration activity decreased indicating that electron transport in the respiratory chain is inhibited by CN^-, which is known to bind strongly to cytochrome oxidase. The effect of exposure of HeLa cells to various chemicals has also been assessed by SECM and the results were compared to fluorescence microscopy (Kaya *et al* 2003) (figure 20).

Using a similar approach to assess respiration as a marker of cell viability, the proliferation and chemosensitivity of collagen-embedded cells to a range of anti-cancer drugs were investigated in a prototype, on-chip, multi-condition assay (Torisawa *et al* 2003, 2004). In these experiments, wells containing a few hundred cells embedded in collagen were microengineered onto a chip. The entire cell chip was incubated in the desired concentration of a drug

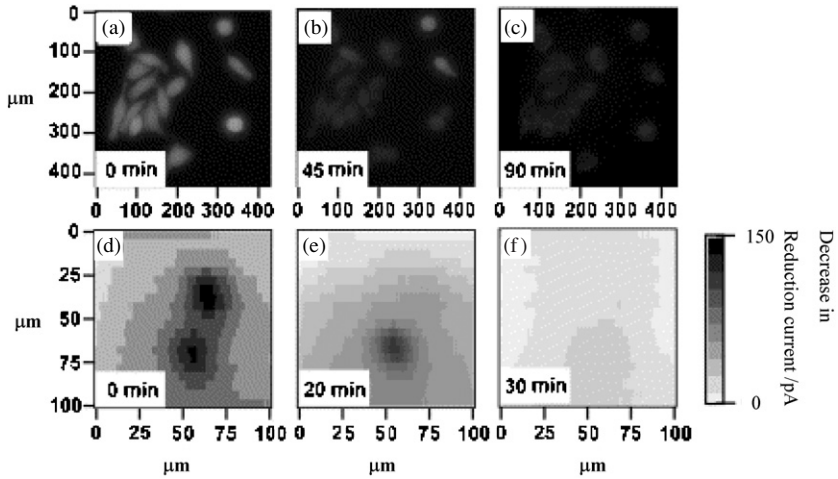

Figure 20. Fluorescence and SECM images of HeLa cells after exposure to 20 mM KCN. Fluorescence images of HeLa cells, taken (a) before and after the exposure to 20 mM KCN for (b) 45 min and (c) 90 min. SECM images of HeLa cells taken (d) before and after the exposure to 20 mM KCN for (e) 20 min and (f) 30 min. A microelectrode, the potential of which was set at −0.50 V versus Ag/AgCl, was scanned at 9.8 μm s^{-1}. (Reproduced with permission from Kaya *et al* (2003), copyright 2003 Elsevier.)

before being transferred to a buffer solution in which the SECM measurements were made. SECM images before and after exposure to the drug clearly indicated a change in the oxygen consumption in the vicinity of the microwells and allowed comparison of the effect of the drug on different cell lines on the same chip. The results were found to tally closely with those measured by a colorimetric assay. The non-invasive nature of the SECM measurement opens up the possibility of continuously monitoring the effect of a dose response. This paves the way for choosing the most effective drug and concentration for treating an individual patient's condition (Torisawa *et al* 2004). A recent development of this biosensor has incorporated a separate microfluidic channel for each cell panel (Torisawa *et al* 2005a, 2005b) to enable different drug exposure conditions to be assessed on the same chip. Recently, a cellular chip has been combined with SECM and enzyme-linked immunosorbant assay (ELISA) as a small volume assay of cytokine release from activated leukocytes (Kasai *et al* 2006)

A similar on-chip system has been developed to assess the respiratory activity of bacterial cells (Kaya *et al* 2001, 2004, Nagamine *et al* 2005a, 2005b). An example of a microchip is shown in figure 21. The metabolic activity of *Escherichia coli* has been investigated by SECM based on the oxygen consumption rate and the reduction of ferricyanide to ferrocyanide (Kaya *et al* 2004). Respiratory activity was reduced by the addition of antibiotics, enabling the determination of minimum inhibitory concentrations (Kaya *et al* 2001). The reduction of ferricyanide by the 'superbug' *Staphylococcus aureus* was assessed using the tip detection mode and found to be enhanced by increased osmotic stress, presumably caused by an increased permeability of the cell membranes or a reorganization of their protein content (Nagamine *et al* 2005a). Assays of ferrocyanide production by *Paracoccus denitrificans* demonstrated that the flow of electrons through the respiratory chain was dependent on the availability of different types of carbon source and the activity of the corresponding catabolite metabolising pathways (Nagamine *et al* 2005b). SECM–microbial chips have also been used to screen for mutagens (Matsui *et al* 2006).

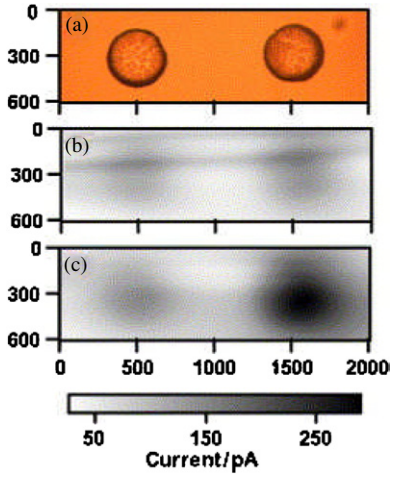

Figure 21. Parallel detection of glucose metabolic regulation in the *P. denitrificans*. (a) An image of the microbial chip with *P. denitrificans* spots precultured with (right spot) and without (left spot) 20.0 mM D-(+)-glucose. The SECM images before (b) and after the addition of 20.0 mM D-(+)-glucose (c). Scan rate = 73.2 μm s^{-1}. (Reproduced with permission from Nagamine *et al* (2005b), copyright 2005 Elsevier.)

In a recent study, the cytotoxic effect of silver(I) on the respiratory chain of *Escherichia coli* was characterized (Holt and Bard 2005). Bacterial cells were immobilized on a glass slide and SECM was used to determine the uptake of Ag^+ by living and dead cells. Ferricyanide was used as an alternative electron acceptor to allow probing of the site of inhibition within the respiratory chain (Holt and Bard 2005).

SECM has also been employed to probe the gradient in oxygen near to a single living bovine embryo (Shiku *et al* 2001, 2004, 2005). Respiratory activity of embryos was found to strongly correlate with the developmental stage and the size of the embryos as determined by optical microscopy (Shiku *et al* 2001, 2004, Agung *et al* 2005), with the morulae (development stage of embryo reached on day 6 after *in vitro* fertilization) with the highest oxygen consumption showing most potential for further development into embryos of larger size.

6.3.3. Cellular redox activity. Measurements of intracellular redox activity performed on large populations of cells typically suffer from slow rates of mass transfer (minute time scale) and valuable information can be lost in the time-averaged signal produced by a large number of cells. In contrast, the time scale of single-cell measurements employing the SECM feedback mode is much faster (milli- to microsecond time scale). The principle of this approach is illustrated in figure 22. The UME is placed in a buffered solution containing a hydrophobic redox mediator, e.g. the oxidized form of a quinone such as 1,4-naphthoquinone (menadione), and is used to electrogenerate the reduced form of the mediator, e.g. menadiol, near to the cell membrane. The product of the tip reaction may penetrate into a cell and undergo a bimolecular reaction with intracellular redox moieties, regenerating the initial species. This species may cross the cell membrane to be detected at the tip resulting in an enhanced tip current flowing at the electrode, i.e. feedback. The concentration of mediator employed in these experiments is of the order of μM to ensure sufficient sensitivity of the approach.

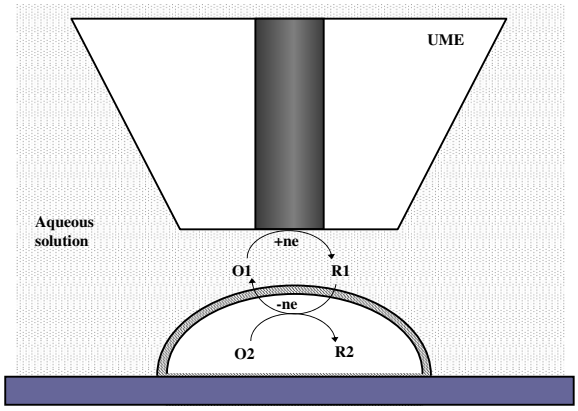

Figure 22. Schematic of the SECM feedback mode applied to study the redox activity of single cells. The oxidized form of the mediator (O1) is generated via a biomolecular ET reaction of R1 with cell-bound redox moieties (O2).

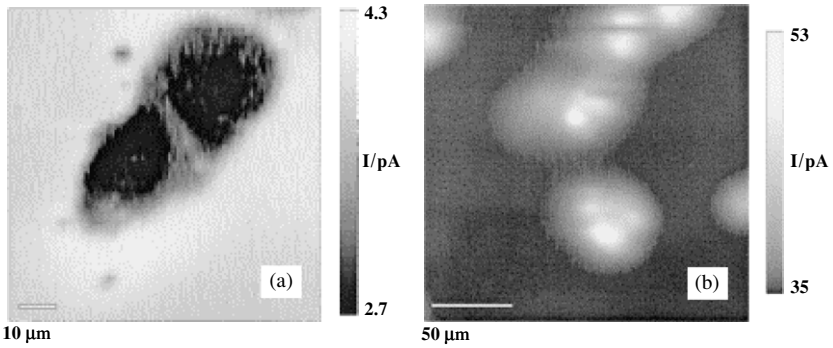

Figure 23. Maps of redox activity in normal (MCF-10A) (a) and metastatic (MDA-MB-231) (b) human breast cells obtained with a hydrophobic redox mediator. The concentration of 1,2-naphthoquinone in solution was (a) 40 μM and (b) 30 μM. A 1 μm radius Pt (a) or 5.5 μm C (b) tip was biased at -0.36 V versus Ag/AgCl and scanned at 10 μm s^{-1}. (Reproduced with permission from Liu *et al* (2001), copyright 2001 Elsevier.)

This technique was first employed by Mirkin *et al* to study the different redox activities of non-metastatic and metastatic human breast cells which express different levels of the enzyme protein kinase Cα (Liu *et al* 2000, 2002, Mirkin *et al* 2002). This enzyme has been linked with motility and metastasis of various cell types. Approach curve measurements using menadione and 1,2-naphthaquinone as mediators demonstrated that the rate of regeneration of the mediator was significantly lower for the metastatic cells expressing high levels of protein kinase Cα. SECM was also used to map the redox activity of an individual cell. Figure 23 shows images of normal and metastatic human breast cells obtained using a hydrophobic mediator, 1,2-naphthoquinone. In the case of the normal cell (figure 23(a)), the region of highest redox activity appears as a bright halo at the cell periphery, whereas the nucleus appears as a dark region which is impenetrable to the redox mediator. With hydrophilic mediators, pure negative feedback was exhibited and so enabled topographic imaging of the cells (Liu *et al* 2001). This type of imaging enabled discrimination between metastatic and

non-metastatic cells (Liu *et al* 2001). Indeed by optimizing cell–electrode distance, cell density, choice of mediator and mediator concentration, discrimination was even achieved when imaging fields of cells containing both metastatic and non-metastatic cells (Feng *et al* 2003, Rotenberg and Mirkin 2004).

The rate of oxidation–reduction reactions of various hydrophobic mediators was probed in greater detail to characterize the differences in redox activity of the metastatic and non-metastatic cells (Liu *et al* 2002). Depending on the experimental conditions used, the overall rate of transmembrane charge transfer may be limited by factors such as mediator potential, intracellular concentration of redox centres or membrane permeability. The results suggested that membrane transfer of a cationic mediator such as *N*,*N*,*N*′,*N*′-tetramethyl-1,4-phenylenediamine was always rate limiting. For the hydrophobic quinone mediators the rate-limiting step shifts from being controlled by membrane transport at low mediator concentrations to being controlled by the rate of generation of redox centres inside the cell at high concentrations. The differences in redox activities of the non-transformed breast cells and metastatic breast cancer cells appeared to arise from different concentrations of the intracellular redox-active moieties.

Cells of the photosynthetic purple bacterium *Rhodobacter sphaeroides* (cell radius 10 μm) have also been studied using this approach (Cai *et al* 2002). *Rhodobacter* was shown to reduce (or oxidize) several hydrophilic species which did not penetrate the membrane of mammalian cells. Matsue and co-workers have investigated the redox activity of a single protoplast by detecting the production of ferriceniummethanol (FMA^+) at an UME tip scanned in seawater containing ferrocenemethanol and hydrogen peroxide. The generation of FMA^+ coupled with H_2O_2 reduction was attributed to a peroxidase-catalyzed reaction within the protoplast (Zhou *et al* 2003, Shiku *et al* 2005). SECM was also used to map peroxidase activity in celery tissue, which indicated that larger amounts of peroxidases are located in particular regions such as around vascular bundles (Zhou *et al* 2001). A potentiometric antimony probe was used to image the pH profile around single cancer cells with the aim of correlating the amount of acid released with metastasis. This type of probe can also be employed in amperometric mode; thus, the same Sb tip was used to locate a cell and measure the tip–sample distance using the tip current response for oxygen reduction in feedback mode (Liu *et al* 2001).

6.3.4. Neurons. The high temporal and spatial resolution of microelectrodes has facilitated the study of exocytosis by single neural cells, where it is possible to detect zeptomolar quantities of neurotransmitter from a single neural vesicle as a transient current spike in the electrode response (Hochstetler *et al* 2000, Amatore *et al* 2005, Wightman 2006).

In recent years, SECM has emerged as a powerful tool for investigating the spatial distribution of neurotransmitter release and the morphology changes of neural cells undergoing differentiation (Hengstenberg *et al* 2001, Liebetrau *et al* 2003, Takii *et al* 2003, Kurulugama *et al* 2005). Using carbon fibre microelectrodes sited above a cellular feature by SECM shear force positioning (section 5.1), it has proven possible to image individual PC12 cells and monitor discrete exocytotic events, releasing catecholamine neurotransmitters upon stimulation with K^+ (Hengstenberg *et al* 2001). Differentiated and undifferentiated PC12 cells were imaged in SECM constant-height feedback mode using several mediators that were selected for their biocompatibility from a larger pool of candidates (Liebetrau *et al* 2003). Exposure of undifferentiated PC12 cells to nerve growth factor induces growth of neurites (long, narrow cell extensions), which were also imaged by SECM. Because neurites are thin structures (1–3 μm diameter) compared to the height of the cell, they posed a particular challenge for imaging. For imaging, the z position of the electrode had to be optimized to make the best use of the sensitivity of the feedback mode at close tip–substrate separations for

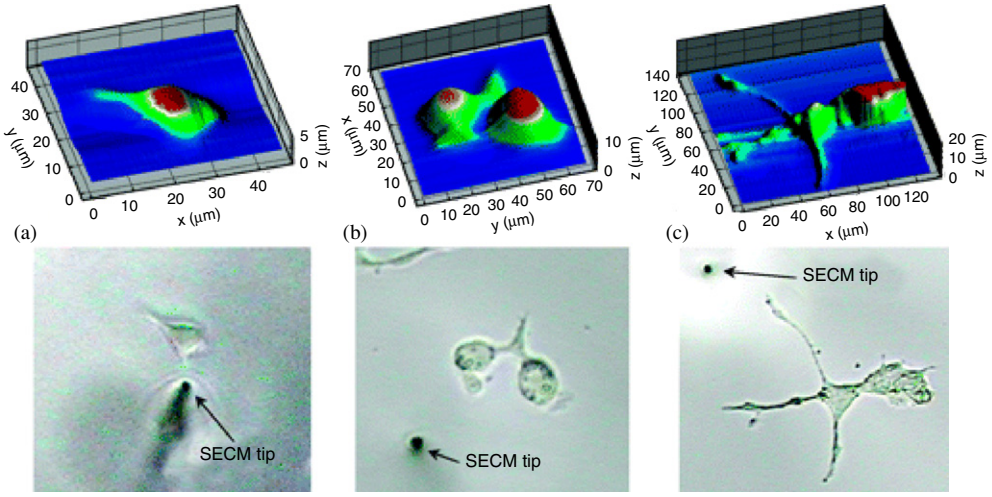

Figure 24. Topographic images acquired using constant-current imaging with a ~1 μm diameter carbon ring electrode. (a) Undifferentiated PC12 cell; (b) PC12 cells in the early stage of neurite development following exposure to NGF; (c) differentiated PC12 cell. Conditions: 1.0 mM $Ru(NH_3)_6^{3+}$ mediator in HBSS, E_T = –0.4 V versus Ag/AgCl, scan rate 5 μm s^{-1} for (a) and 6 μm s^{-1} for (b) and (c). (Reprinted with permission from Kurulugama *et al* (2005), copyright 2005 American Chemical Society.)

the region of interest, whilst preventing contact of the electrode with the sample. The value of using SECM to monitor small changes in cell morphology in real time was exemplified by imaging the reversible change in cell height that is induced by adding hypo/hypertonic solutions (Liebetrau *et al* 2003). Recently, improvements in image resolution have been achieved using constant distance imaging employing two types of feedback signal for distance control—either the electrolysis of a mediator (in constant-current mode) or measurement of the impedance at the SECM tip (in constant-impedance mode). Both approaches were applied to imaging undifferentiated and differentiated PC12 cells. The constant-current mode with a 1 μm diameter carbon ring electrode gave the highest resolution (figure 24); however, the constant-impedance mode also gave improved resolution images compared to constant-height mode. One advantage of the tip impedance based constant-distance mode is that images can be recorded in the growth media without added mediator, facilitating the possibility of long-term imaging during growth and development. By combining amperometry and constant-height impedance, SECM has even allowed simultaneous mapping of topography and detection of vesicular release events while moving the tip across a cell (Kurulugama *et al* 2005). Respiratory activity within single PC12 cells has been studied using SECM measurements of oxygen concentration and it was found that both axons and the cell body were actively consuming oxygen (Takii *et al* 2003). Stimulation of growth by the addition of neuronal growth factor was found to stimulate respiration, particularly in the region of the cells actively forming neurites.

6.3.5. Membrane transport and chemical release. Transport of material across membranes is a fundamental biological process and SECM has been used to study transport processes in a variety of systems (including the release of neurotransmitters by neurons, see above). Recently, SECM has been used to monitor the export of cytotoxic products from living cells (Mauzeroll and Bard 2004, Mauzeroll *et al* 2004). Quinones such as menadione can readily

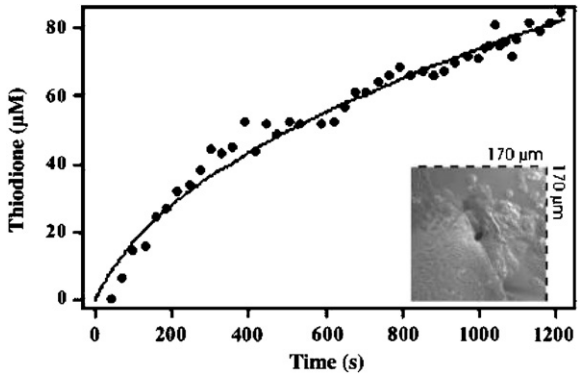

Figure 25. Electrochemical detection of thiodione from highly confluent Hep G2 cells using a 10 μm Pt UME. The potential was scanned from –0.8 to 0.65 V versus Hg/Hg_2SO_4 at a scan rate of 100 mV s^{-1} in deoxygenated 37.5 °C PBS buffer. Dots: the current at 0.5 V versus Hg/Hg_2SO_4 was converted to thiodione concentration and plotted versus the calculated time. Solid line: theoretical fit to experimental data using $D = 4 \times 10^{-6}$ cm^2 s^{-1} and $J = 4.7 \times 10^{-12}$ molecules s^{-1} cm^{-2} and a tip-to-sample distance of 85 μm. (Inset) Optical micrograph of 75–100% confluent liver cells used in these measurements. (Reproduced from Mauzeroll *et al* (2004), copyright 2004 National Academy of Sciences, USA.)

be transported into cells by passive diffusion. Once inside the cell, menadione can generate reactive oxygen species, subjecting the cell to oxidative stress and damage. Several cell types detoxify menadione by converting it to thiodione (menadione–glutathione conjugate), which is then actively transported out of the cell by a protein pump, thought to be involved in the export of chemotherapy drugs by some multi-drug resistance cancer cells. Using yeast as a model organism and hepatocytes, Bard and co-workers have monitored expulsion of thiodione after menadione uptake by oxidation of thiodione at the tip in substrate generation/tip collection mode (Mauzeroll and Bard 2004, Mauzeroll *et al* 2004). Simulations suggested that menadione uptake is the rate-limiting step and the rate of thiodione export was at least an order of magnitude greater in yeast. By monitoring the efflux from a large aggregate of yeast cells (131 cells) immobilized on a glass support, the flux of thiodione was found to be 5.33×10^{-20} mol s^{-1} per cell (Mauzeroll and Bard 2004). The efflux of thiodione represented 10% of the concentration of menadione used to stress the cells indicating that a parallel detoxification mechanism may operate which does not involve transport across the cystolic membrane, such as vacuolar sequestration. The efflux of thiodione was also imaged by SECM for isolated and highly confluent monolayers of hepatoblastoma Hep G2 cells, which are a cell line that expresses high levels of the multi-drug resistant protein (Mauzeroll *et al* 2004). Figure 25 shows the time response of thiodione efflux from highly confluent Hep G2 cells recorded using a 10 μm Pt UME detecting thiodione by oxidation.

Schuhmann *et al* have recently utilized SECM tip detection to amperometrically detect nitric oxide released above growing human umbilical vein endothelial cell (HUVEC) monolayers upon stimulation, using a chemically modified NO-sensing microelectrode (Pailleret *et al* 2003, Isik *et al* 2004, Borgmann *et al* 2006). A dual microelectrode was later employed to facilitate accurate positioning of the NO sensor near to the cell surface, by monitoring changes in the reduction current of oxygen, enabling reproducible and quantitative measurement of activity (Isik *et al* 2004, Borgmann *et al* 2006). Figure 26 shows a typical response of an NO-sensing electrode located at varying distance from the cells. Nitric oxide

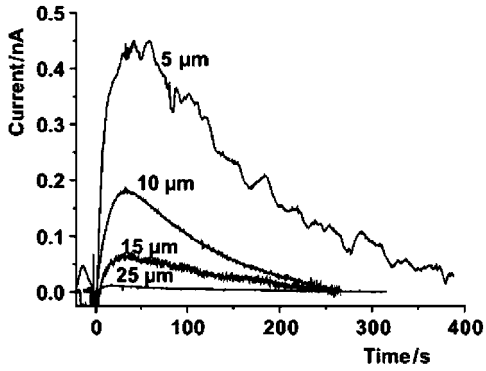

Figure 26. Representative plots of the relative magnitudes of the current signals due to the oxidation of NO recorded at (a) 5, (b) 10, (c) 15 and (d) 25 μm away from the cells. (Reprinted with permission from Isik *et al* (2004), copyright 2004 American Chemical Society.)

levels detected were considerably higher than anticipated based on conventional studies, which was attributed to the fact that SECM measurements probed the near-cell surface environment, and hence were expected to provide a more accurate determination of the short-lived nitric oxide (Pailleret *et al* 2003). Calcium ion selective liquid membrane microelectrodes have been used in the investigation of the release of ionized calcium from bovine cortical bone slices in the presence of osteoclasts, specialized cells responsible for resorption of bone (Berger *et al* 1999). Transport across internal cellular membranes has been assessed in a study of the permeability of the double membrane nuclear envelope of large intact nuclei ($\sim$400 μm diameter) isolated from *Xenopus laevis* oocytes (Guo and Amemiya 2005). SECM approach curve and chronoamperometry measurements were used to determine the permeability coefficients of several ferrocene-derived mediators and indicated that the membrane was freely permeable to the species used. These results suggested that the permeability of the nuclear envelope was at least two orders of magnitude larger than the permeability of bilayer lipid membranes and cell membranes, which was attributed to open nuclear pore complex structures facilitating passive diffusion. The diameter of a nuclear pore complex and the average flux of mediator sustainable by a single pore were estimated by modelling the nuclear envelope as an array of nanometer-sized pores.

7. Conclusions and future perspectives

This review has highlighted numerous and diverse biophysical and biochemical applications of SECM. These include using SECM to measure flow through membranes, investigate local transport properties and measure kinetic parameters of reactions. The impact of micro-electrochemical techniques on the understanding of physicochemical processes at interfaces, including transport across and within bilayers, monolayers, liquid/liquid interfaces and liquid/gas interfaces, has been a significant feature of this review.

We have given several examples of using SECM to make peri-cellular measurements. There are clearly huge prospects for developing this avenue further, particularly for probing single cells, and improving spatial resolution of this type of measurement. There is an impressive body of work on the use of microelectrodes to examine cellular processes at a single-cell level, such as exocytosis (Hochstetler *et al* 2000, Amatore *et al* 2005), redox activity (Liu *et al* 2000) (see section 6.3) and oxidative stress response (Arbault *et al* 2004);

these are reviewed in Wightman (2006). The application of mobile imaging probes, which are the distinguishing feature of SECM and SECM–AFM, should provide enhanced information on processes at single cells.

Many recent technological developments in SECM have arrived from combining it with other physical techniques. SECM–AFM, as considered in sections 2.3.4 and 5.3, has given rise to unparalleled spatial resolution of electrochemical measurements. However, the technique is in its infancy and much more work is necessary, notably the development of reliable methods for mass probe manufacture, to allow it to attain its full potential. Ring electrodes formed around optical fibres have been used to combine photoelectrochemical microscopy (PEM) (James *et al* 1996) and SECM and optical microscopy (SECM/OM) (Lee and Bard 2002). Walsh *et al* (2005) constructed a ring electrode around the opening of a micropipette, to allow the delivery of pl volumes while electrochemically monitoring responses. Other hybrid techniques with SECM that are under development include surface plasmon resonance imaging (SPR-i) (Szunerits *et al* 2004, Fortin *et al* 2005), laser scanning confocal microscopy (Cannan *et al* 2002, Rudd *et al* 2005) and various spectroscopies. The future is expected to see the continuation of this trend, bringing together the strengths of multiple techniques, which have complementary attributes.

A close relative of SECM, using many of the same technologies, is scanning ion conductance microscopy (SICM) (Hansma *et al* 1989, Prater *et al* 1991, Korchev *et al* 1997, Shevchuk *et al* 2001). The scanning probe is an electrolyte-filled micro- or nano-pipette (typical diameter between 50 nm and 1.5 μm). A voltage applied between a reference electrode in solution and an internal electrode (in the pipette) causes an ionic current to flow, the magnitude of which can, after calibration, be used to give the tip-to-surface distance. As well as imaging, the pipette may be used to perform patch clamp measurements at known locations across the cell (Gorelik *et al* 2002). The resolution of SICM, being of the order of the diameter of the pipette (Korchev *et al* 2000), coupled with the ability to image soft samples, without damage, makes this a powerful technique for live cellular imaging. In the future, a marriage of SECM and SICM could produce a very powerful tool, since SECM can selectively detect target molecules including those without a charge.

This review has shown a broad cross section of SECM-based methods and their applications to biological systems. The methodologies are currently at differing stages of maturity, have all shown great promise and in many cases produced new insights into biophysical systems. The future will see SECM applied to many more situations, giving us improved understanding of many biological phenomena, with a likely emphasis on living systems.

References

Agung B, Otoi T, Abe H, Hoshi H, Murakami M, Karji N W K, Murakami M K, Wongsrikeao P, Watari H and Suzuki T 2005 Relationship between oxygen consumption and sex of bovine *in vitro* fertilised embryos *Reprod. Domest. Anim.* **40** 51–6

Amatore C, Arbault S, Bonifas I, Bouret Y, Erard M, Ewing A G and Sombers L A 2005 Correlation between vesicle quantal size and fusion pore release in chromaffin cell exocytosis *Biophys. J.* **88** 4411–20

Amemiya S and Bard A J 2000 Scanning electrochemical microscopy: 40. Voltammetric ion-selective micropipet electrodes for probing ion transfer at bilayer lipid membranes *Anal. Chem.* **72** 4940–8

Amemiya S, Ding Z F, Zhou J F and Bard A J 2000 Studies of charge transfer at liquid/liquid interfaces and bilayer lipid membranes by scanning electrochemical microscopy *J. Electroanal. Chem.* **483** 7–17

Amemiya S, Guo J, Xiong H and Gross D A 2006 Biological applications of scanning electrochemical microscopy: chemical imaging of single living cells and beyond *Anal. Bioanal. Chem.* **386** 458–71

Amman D 1986 *Ion-Selective Microelectrodes: Principles, Design, and Application* (Berlin: Springer)

Arbault S, Sojic N, Bruce D, Amatore C, Sarasin A and Vuillaume M 2004 Oxidative stress in cancer prone xeroderma pigmentosum fibroblasts: real-time and single cell monitoring of superoxide and nitric oxide production with microelectrodes *Carcinogenesis* **25** 509–15

Bach C E, Nichols R J, Meyer H and Besenhard J O 1994 An electropainting method for coating STM tips for electrochemical measurements *Surf. Coat. Technol.* **67** 139–44

Ballesteros-Katemann B and Schuhmann W 2002 Fabrication and characterization of needle-type Pt-disk nanoelectrodes *Electroanalysis* **14** 22–8

Bard A J, Fan F-R F, Kwak J and Lev O 1989 Scanning electrochemical microscopy: introduction and principles *Anal. Chem.* **61** 132–8

Bard A J, Fan F-R F and Mirkin M V 1993 *Electroanalytical Chemistry* vol 18, ed A J Bard (New York: Marcel Dekker) p 243

Bard A J, Fan F-R F and Mirkin M V 1995 *Physical Electrochemistry: Principles, Methods, and Applications* ed I Rubinstein (New York: Marcel Dekker) p 209

Bard A J, Li X and Zhan W 2006 Chemically imaging living cells by scanning electrochemical microscopy *Biosens. Bioelectron.* at press

Bard A J and Mirkin M V 2001 *Scanning Electrochemical Microscopy* (New York: Marcel Dekker)

Bard A J, Mirkin M V, Unwin P R and Wipf D O 1992 Scanning electrochemical microscopy: 12. Theory and experiment of the feedback mode with finite heterogeneous electron-transfer kinetics and arbitrary substrate size *J. Phys. Chem.* **96** 1861–8

Barker A L, Gonsalves M, Macpherson J V, Slevin C J and Unwin P R 1999 Scanning electrochemical microscopy: beyond the solid/liquid interface *Anal. Chim. Acta* **385** 223–40

Barker A L, Macpherson J V, Slevin C J and Unwin P R 1998 Scanning electrochemical microscopy (SECM) as a probe of transfer processes in two-phase systems: theory and experimental applications of SECM-induced transfer with arbitrary partition coefficients, diffusion coefficients and interfacial kinetics *J. Phys. Chem.* B **102** 1586–98

Barker A L, Slevin C J, Unwin P R and Zhang J 2001 *Liquid Interfaces in Chemical, Biological, and Pharmaceutical Applications* ed A G Volkov (New York: Marcel Dekker) p 283

Barnes G T and La Mer V K 1962 *Retardation of Evaporation by Monolayers* ed V K La Mer (New York: Academic) pp 9–33

Barnes G T, Quickenden T I and Saylor J E 1970 Statistical calculation of monolayer permeation by water *J. Colloid Interface Sci.* **33** 236–43

Bath B D, White H S and Scott E R 2001 *Scanning Electrochemical Microscopy* ed A J Bard and M V Mirkin (New York: Marcel Dekker) pp 343–95

Berger C E M, Horrocks B R and Datta H K 1999 Application of ion-selective microelectrodes to the detection of calcium release during bone resorption *Electrochim. Acta* **44** 2677–83

Betzig E, Finn P L and Weiner J S 1992 Combined shear force and near-field scanning optical microscopy *Appl. Phys. Lett.* **60** 2484

Binnig G, Quate C F and Gerber C 1986 Atomic force microscope *Phys. Rev. Lett.* **56** 930–3

Blank M 1964 An approach to a theory of monolayer permeation by gases *J. Phys. Chem.* **68** 2793–800

Blank M and Britten J S 1968 *Physical Principles of Biological Membranes* (New York: Gordon and Breach)

Borden M A and Longo M L 2004 Oxygen permeability of fully condensed lipid monolayers *J. Phys. Chem.* B **108** 6009–16

Borgmann S, Radtke I, Erichsen T, Blöchl A, Heumann R and Schuhmann W 2006 Electrochemical high-content screening of nitric oxide release from endothelial cells *ChemBiolChem.* **7** 662–8

Büchler M, Kelley S C and Smyrl W H 2000 Scanning electrochemical microscopy with shear force feedback. Investigation of the lateral resolution of different experimental configurations *Electrochem. Solid-State Lett.* **3** 35–8

Burt D P, Cervera J, Mandler D, Macpherson J V, Manzanares J A and Unwin P R 2005a Scanning electrochemical microscopy as a probe of Ag^+ binding kinetics at Langmuir phospholipid monolayers *Phys. Chem. Chem. Phys.* **7** 2955–64

Burt D P, Wilson N R, Weaver J M R, Dobson P S and Macpherson J V 2005b Nanowire probes for high resolution combined scanning electrochemical microscopy–atomic force microscopy *Nanoletters* **5** 639–43

Cai C, Liu B, Mirkin M V, Frank H A and Rusling J F 2002 Scanning electrochemical microscopy of living cells: 3. *Rhodobacter sphaeroides Anal. Chem.* **74** 114–9

Cannan S, Douglas Macklam I and Unwin P R 2002 Three-dimensional imaging of proton gradients at microelectrode surfaces using confocal laser scanning microscopy *Electrochem. Commun.* **4** 886–92

Cannan S, Zhang J, Grunfeld F and Unwin P R 2004 Scanning electrochemical microscopy (SECM) studies of oxygen transfer across phospholipid monolayers under surface pressure control: comparison of monolayers at air/water and oil/water interfaces *Langmuir* **20** 701–7

Carlsson S, Liljeroth P and Kontturi K 2005 Channel flow configuration for studying the kinetics of surfactant–polyelectrolyte binding *Anal. Chem.* **77** 6895–901

Ciani I, Burt D P, Daniele S and Unwin P R 2004 Effect of surface pressure on oxygen transfer across molecular monolayers at the air/water interface: scanning electrochemical microscopy investigations using a mercury hemispherical microelectrode probe *J. Phys. Chem.* B **108** 3801–9

Conyers J L Jr and White H S 2001 Electrochemical characterization of electrodes with submicrometer dimensions *Anal. Chem.* **72** 4441–6

Davis J M, Fan F-R F and Bard A J 1987 Currents in thin layer electrochemical cells with spherical and conical electrodes *J. Electroanal. Chem. Interfacial Electrochem.* **238** 9–31

Delville M H, Tsionsky M and Bard A J 1998 Scanning electrochemical microscopy studies of electron transfer through monolayers containing conjugated species at the liquid–liquid interface *Langmuir* **14** 2774–9

Demaille C, Unwin P R and Bard A J 1996 Scanning electrochemical microscopy: 33. Application to the study of ECE/DISP reactions *J. Phys. Chem.* **100** 14137–43

Denuault G, Troise-Frank M H and Peter L M 1992 Scanning electrochemical microscopy: potentiometric probing of ion fluxes *Faraday Discuss. Chem. Soc.* **94** 23–35

Dobson P S, Weaver J M R, Holder M N, Unwin P R and Macpherson J V 2005 Characterization of batch-microfabricated scanning electrochemical–atomic force microscopy probes *Anal. Chem.* **77** 424–34

Donaldson D J and Vaida V 2006 The influence of organic films at the air–aqueous boundary on atmospheric processes *Chem. Rev.* **106** 1445–61

Edidin M 1981 *Membrane Structure* ed J B Finean and R H Michell (New York: Elsevier) p 37

Eftekhari A 2001 Chemical sensor based on silver/silver sulfide microelectrode *Anal. Lett.* **34** 1087–95

Elson E L 1985 Fluorescence correlation spectroscopy and photobleaching recovery *Annu. Rev. Phys. Chem.* **36** 379–406

Elson E L 1986 *Optical Methods in Cell Physiology* ed P D Weer and B M Salzberg (New York: Wiley) p 367

Evans N J, Gonsalves M, Gray N J, Barker A L, Macpherson J V and Unwin P R 2000 Local amperometric detection of K^+ in aqueous solution using scanning electrochemical microscopy ion-transfer voltammetry *Electrochem. Commun.* **2** 201–6

Feldberg S 1972 *Computers in Chemistry, Instrumentation Electrochemistry* vol 2 ed J S Mathson, H B M Jr and H C M Jr (New York: Marcel Dekker) pp 185–215

Feng W J, Rotenberg S A and Mirkin M V 2003 Scanning electrochemical microscopy of living cells: 5. Imaging of fields of normal and metastatic human breast cells *Anal. Chem.* **75** 4148–54

Finkelstein A 1976 Water and nonelectrolyte permeability of lipid bilayer membranes *J. Gen. Physiol.* **68** 127–35

Finkelstein A 1987 *Water Movement Through Lipid Bilayers, Pores, and Plasma Membranes* (New York: Wiley)

Forster R J 2003 *Microelectrodes—Retrospect and Prospect Encyclopedia of Electrochemistry (Instrumentation and Electroanalytical Chemistry* vol 3*)* ed A J Bard, M Stratmann and P R Unwin (New York: Wiley) pp 160–95

Fortin E, Defontaine Y, Mailley P, Livache T and Szunerits S 2005 Micro-imprinting of oligonucleotides and oligonucleotide gradients on gold surfaces: a new approach based on the combination of scanning electrochemical microscopy and surface plasmon resonance imaging (SECM/SPR-i) *Electroanalysis* **17** 495–503

Gabriel B and Teissié J 1991 Proton lateral conduction along lipid monolayers is present only in the liquid-expanded state *J. Am. Chem. Soc.* **113** 8818–21

Gabriel B and Teissié J 1996 Proton long-range migration along protein monolayers and its consequences on membrane coupling *Proc. Natl Acad. Sci. USA* **93** 14521–5

Gardner C E and Macpherson J V 2002 Atomic force microscopy probes go electrochemical *Anal. Chem.* **74** 576A–584A

Gardner C E and Unwin P R 2000 *MChem Report* University of Warwick

Gardner C E, Unwin P R and Macpherson J V 2005 Correlation of membrane structure and transport activity using combined scanning electrochemical–atomic force microscopy *Electrochem. Commun.* **7** 612–8

Gennis R B 1989 *Biomembranes: Molecular Structure* (New York: Springer) p 533

Gewirth A A, Craston D H and Bard A J 1989 Fabrication and characterization of microtips for *in situ* scanning tunneling microscopy *J. Electroanal. Interfacial Chem.* **261** 477–82

Girault H H and Schiffrin D J 1989 *Electroanalytical Chemistry* vol 15 ed A J Bard (New York: Marcel Dekker)

Gonsalves M, Barker A L, Macpherson J V, Unwin P R, O'Hare D and Winlove C P 2000a Scanning electrochemical microscopy as a local probe of oxygen permeability in cartilage *Biophys. J.* **78** 1578–88

Gonsalves M, Macpherson J V, O'Hare D, Winlove C P and Unwin P R 2000b High resolution imaging of the distribution and permeability of methyl viologen dication in bovine articular cartilage using scanning electrochemical microscopy *Biochim. Biophys. Acta* **1524** 66–74

Gorelik J *et al* 2002 Ion channels in small cells and subcellular structures can be studied with a smart patch-clamp system *Biophys. J.* **83** 3296–303

Gray N J and Unwin P R 2000 Simple procedure for the fabrication of silver/silver chloride potentiometric electrodes with micrometer and smaller dimensions: application to scanning electrochemical microscopy *Analyst* **125** 889–93

Guo J and Amemiya S 2005 Permeability of the nuclear envelope of isolated *Xenopus* oocyte nuclei studied by scanning electrochemical microscopy *Anal. Chem.* **77** 2147–56

Guo X, Unwin P R, Whitworth A L and Zhang J 2004 Microelectrochemical techniques for probing kinetics at liquid/liquid interfaces *Prog. React. Kinet. Mech.* **29** 43–166

Gutman M and Nachliel E 1995 The dynamics of proton exchange between bulk and surface groups *Biochim. Biophys. Acta* **1231** 123–38

Gyurcsányia R E, Jágerszkia G, Kiss G and Tóth K 2004 Chemical imaging of biological systems with the scanning electrochemical microscope *Bioelectrochemistry* **63** 207–15

Hanai T, Haydon D A and Taylor J 1964 An investigation by electrical methods of lecithin-in-hydrocarbon films in aqueous solutions *Proc. R. Soc.* A **281** 377–91

Hansma P K, Drake B, Marti O, Gould S A C and Prater C B 1989 The scanning ion-conductance microscope *Science* **243** 641–3

Hengstenberg A, Blöchl A, Dietzel I D and Schuhmann W 2001 Spatially resolved detection of neurotransmitter secretion from individual cells by means of scanning electrochemical microscopy *Angew. Chem. Int. Edn Engl.* **40** 905–8

Hengstenberg A, Kranz C and Schuhmann W 2000 Facilitated tip-positioning and applications of non-electrode tips in scanning electrochemical microscopy using a shear force based constant-distance mode *Chem. Eur. J.* **6** 1547–54

Hewitt G F, Shires G L and Polezhaev Y V 1997 *International Encyclopedia of Heat and Mass Transfer* (Boca Raton, FL: CRC Press)

Hliva P, Kapui I, Nagy G and Czako L 1998 Amperometric bacterial electrode for the selective determination of ammonium ion concentration *Magyar Kemiai Folyoirat* **104** 224–31

Hochstetler S E, Puopolo M, Gustincich S, Raviola E and Wightman R M 2000 Real-time amperometric measurements of zeptomole quantities of dopamine released from neurons *Anal. Chem.* **72** 489–96

Holder M N, Gardner C E, Macpherson J V and Unwin P R 2005 Combined scanning electrochemical–atomic force microscopy (SECM–AFM): simulation and experiment for flux-generation at un-insulated metal-coated probes *J. Electroanal. Chem.* **585** 8–18

Holland R-A B, Shibata H, Scheid P and Piiper J 1985 Kinetics of O_2 uptake and release by red cells in stopped-flow apparatus: effects of unstirred layer *Respir. Physiol.* **59** 71–91

Holt K B and Bard A J 2005 Interaction of silver(I) ions with the respiratory chain of *Escherichia coli*: an electrochemical and scanning electrochemical microscopy study of the antimicrobial mechanism of micromolar Ag^+ *Biochemistry* **44** 13214–23

Horrocks B R, Mirkin M V, Pierce D T, Bard A J, Nagy G and Toth K 1993 Scanning electrochemical microscopy: 19. Ion-selective potentiometric microscopy *Anal. Chem.* **65** 1213–24

Horrocks B R and Wittstock G 2000 *Imaging Cells Under Physiological Conditions in Scanning Electrochemical Microscopy* (New York: Marcel Dekker) pp 445–519

Huebner K J and Thornton E A 1982 *The Finite Element Method for Engineers* 2nd edn (New York: Wiley-Interscience)

Isik S, Etienne M, Oni J, Blöchl A, Reiter S and Schuhmann W 2004 Dual microelectrode for distance control and detection of nitric oxide from endothelial cells by means of scanning electrochemical microscope *Anal. Chem.* **76** 6389–94

James P, Casillas N and Smyrl W H 1996 Simultaneous scanning electrochemical and photoelectrochemical microscopy of pitting sites on titanium *Proc. Electrochem. Soc.* **95** 425–34

James P I, Garfias-Mesias L F, Moyer P J and Smyrl W H 1998 Scanning electrochemical microscopy with simultaneous independent topography *J. Electrochem. Soc.* **145** L64–6

Johnson R W 1998 *The Handbook of Fluid Dynamics* (Boca Raton, FL: CRC Press)

Jones C E, Macpherson J V, Barber Z H, Somekh R E and Unwin P R 1999 Scanning electrochemical microscopy: beyond the solid/liquid interface *Electrochem. Commun.* **1** 55–60

Jones C E, Macpherson J V and Unwin P R 2000 *In situ* observation of the surface processes involved in dissolution from the (0 1 0) surface of potassium ferrocyanide trihydrate in aqueous solution using an integrated electrochemical–atomic force microscope *J. Phys. Chem.* B **104** 2351–9

Jones C E, Unwin P R and Macpherson J V 2003 *In situ* observation of the surface processes involved in dissolution from the cleavage surface of calcite in aqueous solution using combined scanning electrochemical–atomic force microscopy (SECM–AFM) *Chem. Phys. Chem.* **4** 139–46

Kasai S, Shiku H, Torisawa Y S, Nagamine K, Yasukawa T, Watanabe T and Matsue T 2006 Cytokine assay on a cellular chip by combining collagen gel embedded culture with scanning electrochemical microscopy *Anal. Chim. Acta* **566** 55–9

Kaya T, Nishizawa M, Yasukawa T, Nishiguchi M, Onouchi T and Matsue T 2001 A microbial chip combined with scanning electrochemical microscopy *Biotechnol. Bioeng.* **76** 391–4

Kaya T, Numai D, Nagamine K, Aoyagi S, Shiku H and Matsue T 2004 Respiration activity of *Escherichia coli* entrapped in a cone-shaped microwell and cylindrical micropore monitored by scanning electrochemical microscopy (SECM) *Analyst* **129** 529–34

Kaya T, Torisawa Y S, Oyamatsu D, Nishizawa M and Matsue T 2003 Monitoring the cellular activity of a cultured single cell by scanning electrochemical microscopy (SECM): a comparison with fluorescence viability monitoring *Biosens. Bioelectron.* **18** 1379–83

Kemp T J, Unwin P R and Vincze L 1995 Photogenerated chloride ion concentration near the surface of UV-irradiated titanium dioxide in the presence of aqueous 2,4-dichlorophenol probed using an ultramicroelectrode *J. Chem. Soc. Faraday Trans.* **91** 3893–6

Keung A, Kranz C, Lugstein A, Bertagnolli E and Mizaikoff B 2003 Integrated AFM–SECM in tapping mode: simultaneous topographical and electrochemical imaging of enzyme activity *Angew. Chem. Int. Edn Engl.* **42** 3238–40

Keung A, Kranz C, Lugstein A, Bertagnolli E and Mizaikoff B 2005 AFM-tip-integrated amperometric microbiosensors: high-resolution imaging of membrane transport *Angew. Chem. Int. Edn Engl.* **44** 3419–22

Klusmann E and Schultze J W 1997 pH-microscopy—theoretical and experimental investigations *Electrochim. Acta* **42** 3123–34

Korchev Y E, Milovanovic M, Bashford C L, Bennett D C, Sviderskaya E V, Vodyanoy I and Lab M J 1997 Specialized scanning ion-conductance microscope for imaging of living cells *J. Microsc.* **188** 17–23

Korchev Y E, Raval M, Lab M J, Gorelik J, Edwards C R W, Rayment T and Klenerman D 2000 Hybrid scanning ion conductance and scanning near-field optical microscopy for the study of living cells *Biophys. J.* **78** 2675–9

Kranz C, Friedbacher G, Mizaikoff B, Lugstein A, Smoliner J and Bertagnolli E 2001 Integrating an ultramicroelectrode in an AFM cantilever: combined technology for enhanced information *Anal. Chem.* **73** 2491–500

Kranz C, Kueng A, Lugstein A, Bertagnolli E and Mizaikoff B 2004 Mapping of enzyme activity by detection of enzymatic products during AFM imaging with integrated SECM–AFM probes *Ultramicroscopy* **100** 127–34

Kranz C, Ludwig M, Gaub H E and Schuhmann W 1995a Lateral deposition of polypyrrole lines by the scanning electrochemical microscope *Adv. Mater.* **7** 38–40

Kranz C, Ludwig M, Gaub H E and Schuhmann W 1995b High-resolution lateral deposition of polypyrrole as a means for the construction of organic transistors *Adv. Mater.* **7** 568–71

Kranz C, Wittstock G, Wohlschläger H and Schuhmann W 1997 Imaging of microstructured biochemically active surfaces by means of scanning electrochemical microscopy *Electrochim. Acta* **42** 3105–11

Kurulugama R T, Wipf D O, Takacs S A, Pongmayteegul S, Garris P A and Baur J E 2005 Scanning electrochemical microscopy of model neurons: constant distance imaging *Anal. Chem.* **77** 1111–7

Kwak J and Bard A J 1989a Apparatus and two-dimensional scans of conductive and insulating substrates *Anal. Chem.* **61** 1794–9

Kwak J and Bard A J 1989b Scanning electrochemical microscopy: theory of the feedback mode *Anal. Chem.* **61** 1221–7

Langmuir I and Langmuir D B 1927 Effect of monomolecular films on the evaporation of ether solutions *J. Phys. Chem.* **31** 1719–31

Langmuir I and Schaefer V J 1943 Rates of evaporation of water through compressed monolayers on water *J. Franklin Inst.* **235** 119–62

Läuger P 1976 Diffusion-limited ion flow through pores *Biochim. Biophys. Acta* **455** 493–509

Lee Y, Amemiya S and Bard A J 2001 Scanning electrochemical microscopy: 41. Theory and characterization of ring electrodes *Anal. Chem.* **73** 2261–7

Lee Y and Bard A J 2002 Fabrication and characterization of probes for combined scanning electrochemical/optical microscopy experiments *Anal. Chem.* **74** 3626–33

Lee C, Kwak J and Bard A J 1990 Application of scanning electrochemical microscopy to biological samples *Proc. Natl Acad. Sci. USA* **87** 1740–3

Leite V B P, Cavalli A and Oliveira O N J 1998 Hydrogen-bond control of structure and conductivity of Langmuir films *Phys. Rev.* E **57** 6835–9

Liebetrau J M, Miller H M, Baur J E, Takacs S A, Anupunpisit V, Garris P A and Wipf D O 2003 Scanning electrochemical microscopy of model neurons: imaging and real-time detection of morphological changes *Anal. Chem.* **75** 563–71

Liljeroth P, Johans C, Slevin C J, Quinn B M and Kontturi K 2002 Disk-generation/ring-collection scanning electrochemical microscopy: theory and application *Anal. Chem.* **74** 1972–8

Liu B, Cheng W, Rotenberg S A and Mirkin M V 2001 Scanning electrochemical microscopy of living cells: 2. Imaging redox and acid/basic reactivities *J. Electroanal. Chem.* **500** 590–7

Liu H Y, Fan F-R F, Lin C W and Bard A J 1986 Scanning electrochemical and tunneling ultramicroelectrode microscope for high-resolution examination of electrode surfaces in solution *J. Am. Chem. Soc.* **108** 3838–9

Liu B and Mirkin M V 2001 Voltammetry at micro-ITIES *Liquid Interfaces in Chemical, Biological and Pharmaceutical Applications* ed A G Volkov (New York: Marcel Dekker) pp 373–97 chapter i-15

Liu B, Rotenberg A and Mirkin M V 2000 Scanning electrochemical microscopy of living cells: different redox activities of nonmetastatic and metastatic human breast cells *Proc. Natl Acad. Sci. USA* **97** 9855–60

Liu B, Rotenberg S A and Mirkin M V 2002 Scanning electrochemical microscopy of living cells: 4. Mechanistic study of charge transfer reactions in human breast cells *Anal. Chem.* **74** 6340–48

Ludwig M, Kranz C, Schuhmann W and Gaub H E 1995 Topography feedback mechanism for the scanning electrochemical microscope based on hydrodynamic forces between tip and sample *Rev. Sci. Instrum.* **66** 2857–60

Macpherson J V, Beeston M A, Unwin P R, Hughes N P and Littlewood D 1995a Imaging the action of fluid flow blocking agents on dentinal surfaces using the scanning electrochemical microscope *Langmuir* **11** 3959–63

Macpherson J V, Beeston M A, Unwin P R, Hughes N P and Littlewood D 1995b Scanning electrochemical microscopy as a probe of local fluid flow through porous solids: application to the measurement of convective rates through a single dentinal tubule *J. Chem. Soc. Faraday Trans.* **91** 1407–10

Macpherson J V, Jones C E, Barker A L and Unwin P R 2002 Electrochemical imaging of diffusion through single nanoscale pores *Anal. Chem.* **74** 1841–8

Macpherson J V, O'Hare D, Unwin P R and Winlove C P 1997 Quantitative spatially-resolved measurements of mass transfer through laryngeal cartilage *Biophys. J.* **73** 2771–81

Macpherson J V and Unwin P R 1994 A novel approach to the study of dissolution kinetics using the scanning electrochemical microscope: theory and application to the dissolution of $CuSO_4{\cdot}5H_2O$ in aqueous sulfuric acid solutions *J. Phys. Chem.* **98** 1704–13

Macpherson J V and Unwin P R 1995a Scanning electrochemical microscope induced dissolution: rate law and reaction rate imaging for the dissolution of the (0 1 0) face of potassium ferrocyanide trihydrate in non-stoichiometric aqueous solutions of the lattice ions *J. Phys. Chem.* **99** 3338–51

Macpherson J V and Unwin P R 1995b Scanning electrochemical microscopy as a probe of silver chloride dissolution kinetics in aqueous solution *J. Phys. Chem.* **99** 14824–31

Macpherson J V and Unwin P R 1996 Scanning electrochemical microscope induced dissolution: theory and experiment for silver chloride dissolution in aqueous solution without supporting electrolyte *J. Phys. Chem.* **100** 19475–83

Macpherson J V and Unwin P R 1997 Determination of the diffusion coefficient of hydrogen in aqueous solution using single and double potential step chronoamperometry at a disk ultramicroelectrode *Anal. Chem.* **69** 2063–9

Macpherson J V and Unwin P R 2000 Combined scanning electrochemical–atomic force microscopy *Anal. Chem.* **72** 276–85

Macpherson J V and Unwin P R 2001 Noncontact electrochemical imaging with combined scanning electrochemical–atomic force microscopy *Anal. Chem.* **73** 550–7

Macpherson J V and Unwin P R 2005 Scanning electrochemical microscopy as an *in vitro* technique for measuring convective flow rates across dentine and the efficacy of surface blocking treatments *Electroanalysis* **17** 197–204

Macpherson J V, Unwin P R, Hillier A C and Bard A J 1996 *In situ* imaging of ionic crystal dissolution using an integrated electrochemical/AFM probe *J. Am. Chem. Soc.* **118** 6445–52

Mandler D and Unwin P R 2003 Measurement of lateral charge propagation in polyaniline layers with the scanning electrochemical microscope *J. Phys. Chem.* B **107** 407–10

Martin R D and Unwin P R 1997 Scanning electrochemical microscopy: theory and experiment for the positive feedback mode with unequal diffusion coefficients of the redox mediator couple *J. Electroanal. Chem.* **439** 123–36

Martin R D and Unwin P R 1998a Scanning electrochemical microscopy: kinetics of chemical reactions following electron-transfer measured with the substrate generation–tip collection mode *J. Chem. Soc. Faraday Trans.* **94** 753–9

Martin R D and Unwin P R 1998b Theory and experiment for the substrate generation/tip collection mode of the scanning electrochemical microscope: application as an approach for measuring the diffusion coefficient ratio of a redox couple *Anal. Chem.* **70** 276–84

Matsue T, Shiku H, Yamada H and Uchida I 1994 Permselectivity of voltage-gated alamethicin ion channel studied by microamperometry *J. Phys. Chem.* **98** 11001–3

Matsui N, Kaya T, Nagamine K, Yasukawa T, Shiku H and Matsue T 2006 Electrochemical mutagen screening using microbial chip *Biosens. Bioelectron.* **21** 1202–9

Mauzeroll J and Bard A J 2004 Scanning electrochemical microscopy of menadione–glutathione conjugate export from yeast cells *Proc. Natl Acad. Sci. USA* **101** 7862–7

Mauzeroll J, Bard A J, Owhadian O and Monks T J 2004 Menadione metabolism to thiodione in hepatoblastoma by scanning electrochemical microscopy *Proc. Natl Acad. Sci. USA* **101** 17582–7

Menestrina G, Voges K P, Jung G and Boheim G 1986 Voltage-dependent channel formation by rods of helical polypeptides *J. Membr. Biol.* **93** 111–32

Mirkin M V 1999 High-resolution studies of heterogeneous processes with the scanning electrochemical microscope *Mikrochim. Acta* **130** 127–53

Mirkin M V, Fan F-R F and Bard A J 1992 Scanning electrochemical microscopy: 13. Evaluation of the tip shapes of nanometer size microelectrodes *J. Electroanal. Chem.* **328** 47–62

Mirkin M V and Horrocks B R 2000 Electroanalytical measurements using the scanning electrochemical microscope *Anal. Chim. Acta* **406** 119–46

Mirkin M V, Liu B and Rotenberg S A 2002 Probing redox activity of human breast cells by scanning electrochemical microscopy *Methods Enzymol.* **352** 112–22

Möhwald H 1995 *Phospholipid Monolayers Structure and Dynamics of Membranes* vol 1a ed R Lipowsky and E Sackmann (Amsterdam: Elsevier) pp 161–211

Montal M and Mueller P 1972 Formation of bimolecular membranes from lipid monolayers and a study of their electrical properties *Proc. Natl Acad. Sci. USA* **69** 3561–6

Mueller P, Rudin D O, Tien H T and Westcott W C 1963 Methods for the formation of single bimolecular lipid membranes in aqueous solution *J. Phys. Chem.* **67** 534–5

Nachliel E and Gutman M 1988 Time-resolved proton–phospholipid interaction: methodology and kinetic analysis *J. Am. Chem. Soc.* **110** 2629–35

Nagahara L A, Thundat T and Lindsay S M 1989 Preparation and characterization of STM tips for electrochemical studies *Rev. Sci. Instrum.* **60** 3128–30

Nagamine K, Kaya T, Yasukawa T, Shiku H and Matsue T 2005a Application of microbial chip for amperometric detection of metabolic alteration in bacteria *Sensors Actuators* B **108** 676–82

Nagamine K, Matsui N, Kaya T, Yasukawa T, Shiku H, Nakayama T, Nishino T and Matsue T 2005b Amperometric detection of the bacterial metabolic regulation with a microbial array chip *Biosens. Bioelectron.* **21** 145–51

Nugues S and Denuault G 1996 Scanning electrochemical microscopy: amperometric probing of diffusional ion fluxes through porous membranes and human dentin *J. Electroanal. Chem.* **408** 125–40

O'Mullane A P, Macpherson J V, Unwin P R, Cervera-Montesinos J, Manzanares J A, Frehill F and Vos J G 2004 Measurement of lateral charge propagation in $[Os(bpy)_2(PVP)_nCl]Cl$ thin films: a scanning electrochemical microscopy approach *J. Phys. Chem.* B **108** 7219–27

Osborne M C, Shao Y, Pereira C M and Girault H H 1994 Micro-hole interface for the amperometric determination of ionic species in aqueous solutions *J. Electroanal. Chem.* **364** 155–61

Pailleret A, Oni J, Reiter S, Isik S, Etienne M, Bedioui F and Schuhmann W 2003 *In situ* formation and scanning electrochemical microscopy assisted positioning of NO-sensors above human umbilical vein endothelial cells for the detection of nitric oxide release *Electrochem. Commun.* **5** 847–52

Pedley T J 1980 The interaction between stirring and osmosis: part 1 *J. Fluid Mech.* **101** 843–61

Pendley B D and Abruña H D 1990 Construction of submicrometer voltammetric electrodes *Anal. Chem.* **62** 782–4

Penner R M, Heben M J and Lewis N J 1989 Preparation and electrochemical characterization of conical and hemispherical ultramicroelectrodes *Anal. Chem.* **61** 1630–6

Penner R M, Heben M J, Longin T L and Lewis N S 1990 Fabrication and use of nanometer-sized electrodes in electrochemistry *Science* **250** 1118–21

Peters R 1981 Translational diffusion in the plasma membrane of single cells as studied by fluorescence microphotolysis *Cell Biol. Int. Rep.* **5** 733–60

Pierce D T and Bard A J 1993 Scanning electrochemical microscopy: 23. Retention localization of artificially patterned and tissue-bound enzymes *Anal. Chem.* **65** 3598–604

Pierce D T, Unwin P R and Bard A J 1992 Scanning electrochemical microscopy: 17. Studies of enzyme–mediator kinetics for membrane- and surface-immobilized glucose oxidase *Anal. Chem.* **64** 1795–804

Pohl P, Rokitskaya T, Pohl E E and Saparov S M 1997 Permeation of phloretin across bilayer lipid membranes monitored by dipole potential and microelectrode measurements *Biochim. Biophys. Acta* **1323** 163–72

Pohl P and Saparov S M 2000 Solvent drag across gramicidin channels demonstrated by microelectrodes *Biophys. J.* **78** 2426–34

Pohl P, Saparov S M and Antonenko Y N 1998a The size of the unstirred layer as a function of the solute diffusion coefficient *Biophys. J.* **75** 1403–9

Pohl P, Saparov S M, Pohl E E, Evtodienko V Y, Agapov I I and Tonevitsky A G 1998b Dehydration of model membranes induced by lectins from ricinus communis and viscum album *Biophys. J.* **75** 2868–76

Potje-Kamloth K, Janata J and Josowicz M 1989 Electrochemically prepared insulation for carbon-fiber microelectrodes *Ber. Bunsenges. Phys. Chem.* **93** 1480–5

Prater C B, Hansma P K, Tortonese M and Quate C F 1991 Improved scanning ion-conductance microscope using microfabricated probes *Rev. Sci. Instrum.* **62** 2634–8

Prats M, Teissié J and Tocanne J F 1986 Lateral proton conduction at lipid–water interfaces and its implications for the chemiosmotic-coupling hypothesis *Nature* **322** 756–8

Pu G, Longo M L and Borden M A 2005 Effect of microstructure on molecular oxygen permeation through condensed phospholipid monolayers *J. Am. Chem. Soc.* **127** 6524–5

Rao S S 1982 *The Finite Element Method in Engineering* (New York: Pergamon)

Rotenberg S A and Mirkin M V 2004 Scanning electrochemical microscopy: detection of human breast cancer cells by redox environment *J. Mammary Gland Biol. Neoplasia* **9** 375–82

Rothblat G H, Mahlberg F H, Johnson W J and Phillips M C 1992 Apolipoproteins, membrane cholesterol domains, and the regulation of cholesterol efflux *J. Lipid Res.* **33** 1091–7

Rudd N C, Cannan S, Bitziou E, Ciani I, Whitworth A L and Unwin P R 2005 Fluorescence confocal laser scanning microscopy as a probe of pH gradients in electrode reactions and surface activity *Anal. Chem.* **77** 6205–17

Rugar D and Hansma P K 1990 Atomic force microscopy *Phys. Today* **43** 23–30

Schwarzenbach R P, Gschwend P M and Imboden D M 1993 *Environmental Organic Chemistry* (New York: Wiley)

Selzer Y and Mandler D 2000 Integrating an ultramicroelectrode in an AFM cantilever: combined technology for enhanced information *Anal. Chem.* **72** 2383–90

Shao Y and Mirkin M V 1997 Scanning electrochemical microscopy (SECM) of facilitated ion transfer at the liquid/liquid interface *J. Electroanal. Chem.* **439** 137–43

Shao Y and Mirkin M V 1998 Probing ion transfer at the liquid/liquid interface by scanning electrochemical microscopy (SECM) *J. Phys. Chem.* B **102** 9915–21

Shao Y, Mirkin M V, Fish G, Kokotov S, Palanker D and Lewis A 1997 Nanometer-sized electrochemical sensors *Anal. Chem.* **69** 1627–34

Shevchuk A I, Gorelik J, Harding S E, Lab M J, Klenerman D and Korchev Y E 2001 Simultaneous measurement of Ca^{2+} and cellular dynamics: combined scanning ion conductance and optical microscopy to study contracting cardiac myocytes *Biophys. J.* **81** 1759–64

Shiku H, Hara Y, Takeda T, Matsue T and Uchida I 1997 *Solid–Liquid Electrochemical Interfaces* ed G Jerkiewicz, M P Soriaga, K Uosaka and A Wieckowski (Washington, DC: American Chemical Society) pp 202–10

Shiku H, Matsue T and Uchida I 1996 Detection of microspotted carcinoembryonic antigen on a glass substrate by scanning electrochemical microscopy *Anal. Chem.* **68** 1276–8

Shiku H, Shiraishi T, Aoyagi S, Utsumi Y, Matsudaira M, Abe H, Hoshi H, Kasai S, Ohya H and Matsue T 2004 Respiration activity of single bovine embryos entrapped in a cone-shaped microwell monitored by scanning electrochemical microscopy *Anal. Chim. Acta* **522** 51–8

Shiku H, Shiraishi T, Ohya H, Matsue T, Abe H, Hoshi H and Kobayashi M 2001 Oxygen consumption of single bovine embryos probed by scanning electrochemical microscopy *Anal. Chem.* **73** 3751–8

Shiku H, Takeda T, Yamada H, Matsue T and Uchida I 1995 Microfabrication and characterization of diaphorase-patterned surfaces by scanning electrochemical microscopy *Anal. Chem.* **67** 312–7

Shiku H, Torisawa Y S, Takagi A, Aoyagi S, Abe H, Hoshi H, Yasukawa T and Matsue T 2005 Metabolic and enzymatic activities of individual cells, spheroids and embryos as a function of the sample size *Sensors Actuators* B **108** 597–602

Sklyar O, Keung A, Kranz C, Mizaikoff B, Lugstein A, Bertagnolli E and Wittstock G 2005 Numerical simulation of scanning electrochemical microscopy experiments with frame-shaped integrated atomic force microscopy–SECM probes using the boundary element method *Anal. Chem.* **77** 764–71

Slevin C J, Gray N J, Macpherson J V, Webb M A and Unwin P R 1999 Fabrication and characterisation of nanometre-sized platinum electrodes for voltammetric analysis and imaging *Electrochem. Commun.* **1** 282–8

Slevin C J, Macpherson J V and Unwin P R 1997 Measurement of local reactivity at liquid/solid, liquid/liquid and liquid/gas interfaces with the scanning electrochemical microscope: principles, theory and applications of the double potential step chronoamperometric mode *J. Phys. Chem.* B **101** 10851–9

Slevin C J, Ryley S, Walton D J and Unwin P R 1998 A new approach for measuring the effect of a monolayer on molecular transfer across an air/water interface using scanning electrochemical microscopy *Langmuir* **14** 5331–4

Slevin C J, Umbers J A, Atherton J H and Unwin P R 1996 A new approach to the measurement of transfer rates across immiscible liquid/liquid interfaces *J. Chem. Soc. Faraday Trans.* **92** 5177–80

Slevin C J and Unwin P R 2000 Lateral proton diffusion rates along stearic acid monolayers *J. Am. Chem. Soc.* **122** 2597–602

Solomon T and Bard A J 1995 Scanning electrochemical microscopy: 30. Application of glass micropipet tips and electron transfer at the interface between two immiscible electrolyte solutions for SECM imaging *Anal. Chem.* **67** 2787–90

Strutwolf J, Zhang J, Barker A L and Unwin P R 2001 Effect of phospholipids on the kinetics of dioxygen transfer across a 1,2-dichloroethane/water interface *Phys. Chem. Chem. Phys.* **3** 5553–8

Szunerits S, Knorr N, Calemczuk R and Livache T 2004 New approach to writing and simultaneous reading of micropatterns: combining surface plasmon resonance imaging with scanning electrochemical microscopy (SECM) *Langmuir* **20** 9236–41

Takii Y, Takoh K, Nishizawa M and Matsue T 2003 Characterization of local respiratory activity of PC12 neuronal cell by scanning electrochemical microscopy *Electrochim. Acta* **48** 3381–5

Teissié J, Gabriel B and Prats M 1993 Lateral communication by fast proton conduction: a model membrane study *Trends Biochem. Sci.* **18** 243–6

Teissié J, Prats M, Soucaille P and Tocanne F 1985 Evidence for conduction of protons along the interface between water and a polar lipid monolayer *Proc. Natl Acad. Sci. USA* **82** 3217–21

Thibodeaux L J 1996 *Environmental Chemodynamics: Movement of Chemicals in Air, Water, and Soil* 2nd edn (New York: Wiley)

Tien H T 1974 *Bilayer Lipid Membranes (BLM): Theory and Practise* (New York: Marcel Dekker)

Tien H T and Diana A L 1967 Black lipid membranes in aqueous media: the effect of salts on electrical properties *J. Colloid Interface Sci.* **24** 287–96

Torisawa Y S, Kaya T, Takii Y, Oyamatsu D, Nishizawa M and Matsue T 2003 Scanning electrochemical microscopy-based drug sensitivity test for a cell culture integrated in silicon microstructures *Anal. Chem.* **75** 2154–58

Torisawa Y, Shiku H, Kasai S, Nishizawa M and Matsue T 2004 Proliferation assay on a silicon chip applicable for tumors extirpated from mammalians *Int. J. Cancer* **109** 302–8

Torisawa Y-S, Shiku H, Yasukawa T, Nishizawa M and Matsue T 2005a Multi-channel 3D cell culture device integrated on a silicon chip for anticancer drug sensitivity test *Biomaterials* **26** 2165–72

Torisawa Y S, Shiku H, Yasukawa T, Nishizawa M and Matsue T 2005b Three-dimensional micro-culture system with a silicon-based cell array device for multi-channel drug sensitivity test *Sensors Actuators* B **108** 654–9

Tsionsky M, Bard A J and Mirkin M V 1997a Long-range electron transfer through a lipid monolayer at the liquid/liquid interface *J. Am. Chem. Soc.* **119** 10785–92

Tsionsky M, Cardon Z G, Bard A J and Jackson R B 1997b Photosynthetic electron transport in single guard cells as measured by scanning electrochemical microscopy *Plant Physiol.* **113** 895–901

Tsionsky M, Zhou J, Amemiya S, Fan F-R F and Bard A J 1999 Scanning electrochemical microscopy: 38. Application of SECM to the study of charge transfer through bilayer lipid membranes *Anal. Chem.* **71** 4300–5

Turcu F, Schulte A, Hartwich G and Schuhmann W 2004 Imaging immobilised ssDNA and detecting DNA hybridisation by means of the repelling mode of scanning electrochemical microscopy (SECM) *Biosens. Bioelectron.* **20** 925–32

Unwin P R and Bard A J 1991 Scanning electrochemical microscopy: 9. Theory and application of the feedback mode to the measurement of following chemical reaction rates in electrode processes *J. Phys. Chem.* **95** 7814–24

Unwin P R and Bard A J 1992 Scanning electrochemical microscopy: 14. SECM induced desorption: a new technique for the measurement of adsorption/desorption kinetics and surface diffusion rates at the solid/liquid interface *J. Phys. Chem.* **96** 5035–45

Unwin P R, Macpherson J V, Beeston M A, Evans N J, Hughes N P and Littlewood D 1997 New electrochemical techniques for probing phase transfer dynamics at dental interfaces *in vitro Adv. Dent. Res.* **11** 548–59

Vaz W L C, Derzko Z I and Jacobson K A 1982 Photobleaching measurements of the lateral diffusion of lipids and proteins in artificial phospholipid bilayer membranes *Cell. Surf. Rev.* **8** 83–135

Volkov A G, Deamer D W, Tanelian D L and Markin S 1998 *Liquid Interfaces in Chemistry and Biology* (New York: Marcel Dekker)

Walsh D A, Fernández J L, Mauzeroll J and Bard A J 2005 Scanning electrochemical microscopy: 55. Fabrication and characterization of micropipet probes *Anal. Chem.* **77** 5182–8

Wei C, Bard A J, Nagy G and Toth K 1995 Scanning electrochemical microscopy: 28. Ion-selective neutral carrier-based microelectrode potentiometry *Anal. Chem.* **67** 1346–56

White H S and Scott E R 1993 Iontophoretic transport through porous membranes using scanning electrochemical microscopy: application to *in vivo* studies of ion fluxes through skin *Anal. Chem.* **65** 1537–45

Wiesendanger R 1994 *Scanning Probe Microscopy and Spectroscopy* (Cambridge: Cambridge University Press)

Wightman R M 2006 Probing cellular chemistry in biological systems with microelectrodes *Science* **311** 1570–4

Wightman R M and Wipf D O 1989 *Electroanalytical Chemistry* vol 15 ed A J Bard (New York: Marcel Dekker) pp 267–353

Wijayawardhana C A, Wittstock G, Halsall H B and Heineman W R 2000 Spatially addressed deposition and imaging of biochemically active bead microstructures by scanning electrochemical microscopy *Anal. Chem.* **72** 333–8

Wipf D O and Bard A J 1992 Scanning electrochemical microscopy: 15. Improvements in imaging via tip-position modulation and lock-in detection *Anal. Chem.* **64** 1362–7

Wipf D O and Bard A J 1993 Scanning electrochemical microscopy: 21. Constant-current imaging with an autoswitching controller *Anal. Chem.* **65** 1373–7

Wittstock G and Schuhmann W 1997 Formation and imaging of microscopic enzymatically active spots on an alkanethiolate-covered gold electrode by scanning electrochemical microscopy *Anal. Chem.* **69** 5059–66

Wittstock G, Yu K, Halsall H B, Ridgway T H and Heineman W R 1995 Imaging of immobilized antibody layers with scanning electrochemical microscopy *Anal. Chem.* **67** 3578–82

Yamada H, Matsue T and Uchida I 1991 A microvoltammetric study of permeation of ferrocene derivatives through a planer bilayer lipid membrane *Biochem. Biophys. Res. Commun.* **180** 1330–4

Yasukawa T, Kanaya N, Mandler D and Matsue T 2000a Imaging of diaphorase micropatterned at gold arrays with scanning electrochemical microscopy *Chem. Lett.* **5** 458–9

Yasukawa T, Kaya T and Matsue T 1999a Dual imaging of topography and photosynthetic activity of a single protoplast by scanning electrochemical microscopy *Anal. Chem.* **71** 4637–41

Yasukawa T, Kaya T and Matsue T 2000b Characterization and imaging of single cells with scanning electrochemical microscopy *Electroanalysis* **12** 653–9

Yasukawa T, Kondo Y, Uchida I and Matsue T 1998 Imaging of cellular activity of single cultured cells by scanning electrochemical microscopy *Chem. Lett.* 767–8

Yasukawa T, Uchida I and Matsue T 1999b Microamperometric measurements of photosynthetic activity in a single algal protoplast *Biophys. J.* **76** 1129–35

Zaumseil J, Wittstock G, Bahrs S and Steinrücke P 2000 Imaging the activity of nitrate reductase by means of a scanning electrochemical microscope *Fresenius J. Anal. Chem.* **367** 352–5

Zhang J, Barker A L and Unwin P R 2000 Microelectrochemical studies of charge transfer at the interface between two immiscible electrolyte solutions: electron transfer from decamethyl ferrocene to aqueous oxidants *J. Electroanal. Chem.* **483** 95–107

Zhang J, Slevin C J, Morton C, Scott P, Walton D J and Unwin P R 2001 A new approach for measuring lateral diffusion in Langmuir monolayers by scanning electrochemical microscopy (SECM): theory and application *J. Phys. Chem.* B **105** 11120–30

Zhang J, Strutwolf J, Cannan S and Unwin P R 2003 Combined scanning electrochemical microscopy–Langmuir trough technique for investigating phase transfer kinetics across liquid/liquid interfaces modified by a molecular monolayer *Electrochem. Commun.* **5** 105–10

Zhang J and Unwin P R 2002a Proton diffusion at phospholipid assemblies *J. Am. Chem. Soc.* **124** 2379–83

Zhang J and Unwin P R 2002b Scanning electrochemical microscopy (SECM) feedback approach for measuring lateral proton diffusion in Langmuir monolayers: theory and application *Phys. Chem. Chem. Phys.* **4** 3814–9

Zhang J and Unwin P R 2002c Effect of fatty alcohol monolayers on the rate of bromine transfer across the water/air interface: assessment of candidate models using scanning electrochemical microscopy *Langmuir* **18** 1218–24

Zhang J and Unwin P R 2002d Kinetics of $IrCl_6^{2-}$ ion transfer across the water/1,2-dichloroethane interface and the effect of a phospholipid monolayer *Langmuir* **18** 2313–8

Zhang J and Unwin P R 2003 Kinetics of bromine transfer across Langmuir monolayers of phosphatidylethanolamines at the water/air interface *Phys. Chem. Chem. Phys.* **5** 3979–83

Zhang B and Wang E 1994 Fabrication of STM tips with controlled geometry by electrochemical etching and ECSTM tips coated with paraffin *Electrochim. Acta* **39** 103–6

Zhang B, Zhang Y and White H S 2004 The nanopore electrode *Anal. Chem.* **76** 6229–38

Zhou H, Kasai S, Noda H, Ohya-Nishiguchi H, Shiku H and Matsue T 2003 Characterization of the peroxidase activity of single algae protoplasts by scanning electrochemical microscopy *Bull. Chem. Soc. Japan* **76** 1757–62

Zhou H, Kasai S and Yasukawa T 1999 Imaging the activity of immobilized horseradish peroxidase with scanning electrochemical/chemiluminescence microscopy *Electrochemistry* **67** 1135–7

Zhou H, Shiku H, Kasai S, Noda H, Matsue T, Ohya-Nishiguchi H and Kamada H 2001 Mapping peroxidase in plant tissues by scanning electrochemical microscopy *Bioelectrochemistry* **54** 151–6

Zhou F, Unwin P R and Bard A J 1992 Scanning electrochemical microscopy: 16. Study of second-order homogeneous kinetics via the feedback and generation/collection modes *J. Phys. Chem.* **96** 4917–24

Zhu R K, Macfie S M and Ding Z F 2005 Cadmium-induced plant stress investigated by scanning electrochemical microscopy *J. Exp. Bot.* **56** 2831–8

Zoski C G 2002 Ultramicroelectrodes: design, fabrication, and characterization *Electroanalysis* **14** 1041–51